

HAZMAT II: Ultraviolet Variability of Low-Mass Stars in the GALEX Archive

Brittany E. Miles^{1,2,3,4}
 bmiles@ucsc.edu
 and
 Evgenya L. Shkolnik⁵

ABSTRACT

The ultraviolet (UV) light from a host star influences a planet’s atmospheric photochemistry and will affect interpretations of exoplanetary spectra from future missions like the James Webb Space Telescope. These effects will be particularly critical in the study of planetary atmospheres around M dwarfs, including Earth-sized planets in the habitable zone. Given the higher activity levels of M dwarfs compared to Sun-like stars, time resolved UV data are needed for more accurate input conditions for exoplanet atmospheric modeling. The Galaxy Evolution Explorer (*GALEX*) provides multi-epoch photometric observations in two UV bands: near-ultraviolet (NUV; 1771 – 2831 Å) and far-ultraviolet (FUV; 1344 – 1786 Å). Within 30 pc of Earth, there are 357 and 303 M dwarfs in the NUV and FUV bands, respectively, with multiple *GALEX* observations. Simultaneous NUV and FUV detections exist for 145 stars in both *GALEX* bands. Our analyses of these data show that low-mass stars are typically more variable in the FUV than the NUV. Median variability increases with later spectral types in the NUV with no clear trend in the FUV. We find evidence that flares increase the FUV flux density far more than the NUV flux density, leading to variable FUV to NUV flux density ratios in the *GALEX* bandpasses. The ratio of FUV to NUV flux is important for interpreting the presence of atmospheric molecules in planetary atmospheres such as oxygen and methane as a high FUV to NUV ratio may cause false-positive biosignature detections. This ratio of flux density in the *GALEX* bands spans three orders of magnitude in our sample, from 0.008 to 4.6, and is 1 to 2 orders of magnitude higher than for G dwarfs like the Sun. These results characterize the UV behavior for the largest set of low-mass stars to date.

1. Introduction

M dwarfs provide excellent laboratories for understanding the diversity of exoplanets as they represent 75% of the stars in the Milky Way (Bochanski et al. 2010) and are prime targets for

finding small, habitable zone (HZ), rocky exoplanets. An Earth-sized planet in the HZ around an M-type star produces deeper transits and has a shorter follow-up time compared to a HZ planet orbiting a G type star. Using four years of Kepler data, modeling, and follow-up observations, Dressing & Charbonneau (2015) estimated that on average there are at least two small planets around every M dwarf, with at least one Earth-size HZ planet for every seven M dwarfs. In fact, a $>1.3 M_{\oplus}$ planet has been found orbiting in the HZ of our nearest neighbor, mid-M dwarf Proxima Centauri (Anglada-Escudé et al. 2016) and three Earth-sized HZ planets have been found around

¹Department of Astronomy and Astrophysics, University of California, Santa Cruz

²Department of Physics and Astronomy, University of California, Los Angeles

³Lowell Observatory

⁴Department of Physics and Astronomy, Northern Arizona University

⁵School of Earth and Space Exploration, Arizona State University

the late-M star TRAPPIST-1 (Gillon et al. 2017).

Despite all this, M dwarfs come with complications to characterizing exoplanets. For example, the deep convective zones of low-mass stars create non-uniform magnetic fields that rise above the stellar surface, expelling a large amount of energy in the chromosphere and corona. This energy bombards exoplanets with short-wavelength photons and high-energy particles from stellar winds. With such exposure to a variable and energetic environment, one cannot characterize an exoplanet’s atmosphere and habitability without considering the full impact of the host star.

Several teams are studying the atmospheric response of planets exposed to strong emission and variability in the UV and X-ray as they are the most damaging wavelengths to atmospheric photochemistry (e.g. Miguel & Kaltenecker 2014; Rugheimer et al. 2015; Luger et al. 2015; Luger & Barnes 2015; Arney et al. 2016). Models that use real UV spectra (e.g. France et al. 2013) show that detecting and understanding the sources of oxygen gas and other molecules requires knowing the depletion rate and ozone (O₃) build-up caused by the high-energy radiation from the host star. This is especially true when molecular lines are being used to infer biological processes (Rugheimer et al. 2015; Luger & Barnes 2015).

In an extreme case, Segura et al. (2010) investigated the effect of the strongest UV flare (10³³ - 10³⁴ ergs) observed from the very active M dwarf, AD Leo, on the atmosphere of an Earth-like planet in the HZ. They observed a several orders of magnitude decrease in upper-atmosphere O₃ and water abundances within a day with smaller scale fluctuations leading to equilibrium over the course of a year following the flaring event. Even for stars deemed “inactive”, due to the lack of H α emission, time-tagged Hubble Space Telescope (*HST*) UV spectra from four M dwarf planet hosts displayed changes in emission lines ranging from 50 - 500% on the order of minutes (France et al. 2013; Loyd & France 2014).

For stars that are K7 or later, the published relationships between contemporaneous UV bands and variability are limited to samples of less than 10 stars (Mittra-Kraev et al. 2005; France et al. 2016). Monitoring programs for a large sample of M dwarfs are challenging to execute with *HST* and there are limited resources for studying these

objects at very short wavelengths. Measuring the UV flux from M dwarfs needs to be extended to a significantly larger sample of stars to understand the full range of emission levels and variability.

The space-based telescope Galaxy Evolution Explorer (*GALEX*, Morrissey et al. 2005) provides the opportunity to study a much larger sample of M dwarfs than has been possible before. Operational from 2003 to 2012, *GALEX* tiled over 2/3 of the sky with two UV filters, often simultaneously, with 1.2°-diameter images, capturing UV data for hundreds of low-mass stars. The near-ultraviolet (NUV; 1771 – 2831 Å) and far-ultraviolet (FUV; 1344 – 1786 Å) bands are excellent probes for high energy stellar activity because they are composed of emission lines formed in the chromosphere and corona of stars (Kretzschmar et al. 2009; Welsh et al. 2006). Previous variability studies have been conducted with *GALEX*, but focus on a small set of low-mass stars (Wheatley et al. 2008). In this second paper of **H**Abitable **Z**ones and **M**dwarf **A**ctivity across **T**ime (HAZMAT) series, we use archived data from both *GALEX* photometric bands to measure the variability of 376 low-mass stars with spectral types ranging from K7 to M7, and analyze the relationship between the NUV and FUV emission for simultaneous and time-resolved observations.

2. Low-Mass Star Sample and *GALEX* Data

Our target list consisted of 1124 low-mass stars with photometric distances out to 25 pc of Earth assuming field ages (Reid et al. 2007). Once accounting for the young stars in the sample whose distances are in fact slightly further, all targets are within 30 pc. Ages were primarily taken from the HAZMAT I paper, Shkolnik & Barman (2014) and Stelzer et al. (2013) and when available parallactic distances were compiled from Shkolnik et al. (2009), Shkolnik et al. (2012) and the Hipparcos catalogue (Perryman et al. 1997).

Most of the spectral type identifications are from Reid et al. (2007) and these identifications were then confirmed with a literature search. If no spectral identification was available from the original list, a literature measurement is taken with a preference for optical identifications. There are sometimes discrepancies between published stel-

lar types, therefore measurements from large surveys such as the Palomar/MSU survey (Reid et al. 1995, Hawley et al. (1996)) and Meeting the Cool Neighbors Series (Reid & Cruz 2002) are primarily used for consistency. All references for spectral types are listed in Table 1. The seven stars with an “M:” spectral type designation either do not have a literature measurement or have discrepant published values with a > 1 spectral type subclass difference. These stars are excluded from the analysis regarding spectral type and *GALEX* band correlations.

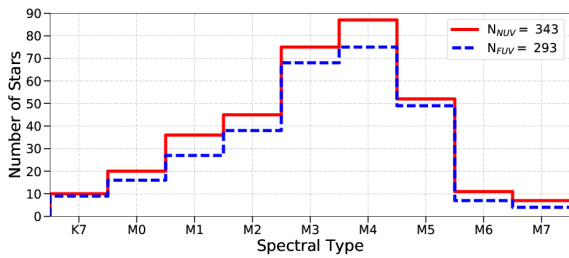


Fig. 1.— The distribution of spectral types for stars with multiple NUV (red) and FUV (blue) observations including $\geq 2\sigma$ detections and upper limits.

TABLE 1
LOW-MASS STARS WITH MULTIPLE GALEX UV OBSERVATIONS

Name ^a	RA J2007 (deg)	DEC J2007 (deg)	SpT	Age ^b (Myr)	Ref	Dist. (pc)	NUV det ^c , u.l.d	NUV μ^e (μJy)	NUV Min,Max ^g (μJy), (μJy)	NUV MAD rel ^f	FUV det ^c , u.l.d	FUV μ^e (μJy)	FUV Min,Max ^g (μJy), (μJy)	FUV MAD rel ^f
LHS1014	1.29780	+45.78628	M1	5000	-1	11.5	2,-	158.26±9.16	145.40,171.13	0.08	-,-	-	-	-
NLTT400	2.36060	-4.13416	M2.5	5000	-12	23.8	6,-	78.76±5.15	69.28,94.54	0.07	-,-	24.61±1.23	7.76,17.84	0.56
NLTT557	2.97127	-22.98422	M3.5	2000	14.1	16.0	2,-	16.43±3.45	12.34,22.89	0.12	-2	≤ 39.21	-	0.54
00144767-6003477	3.69901	-60.06337	M3.5	4000	7.7	25.1	2,-	438.25±25.23	298.25,578.29	0.31	-2	90.60±18.72	62.69,118.50	0.31
GJ1005	3.86861	-16.13497	M4	5000	-1	5.0	2,-	1.74±0.43	1.01,2.47	0.42	-2	≤ 1.49	-	0.10
GJ3017	3.90328	-29.76701	M4	5000	-2	18.1	2,-	87.22±10.26	62.57,111.85	0.28	1,1	22.06±4.13	0.00,0.00	0.20
LHS1051	3.96802	-67.99805	M0.5	5000	-2	19.8	2,-	153.51±4.46	144.19,162.85	0.06	-,-	-	-	-
GJ3030	5.49148	+49.21050	M2.4	150	13.1	24.8	2,-	400.83±27.59	326.46,475.24	0.19	1,1	81.64±14.49	43.48,119.81	0.47
GJ3033	6.14622	+30.04158	M4.5	5000	-2	19.0	2,-	45.10±8.14	42.06,48.16	0.33	0,7	26.89±6.12	18.12,35.67	0.33
G132-4	8.36566	+36.84086	M3	5000	-1	19.1	3,-	34.65±6.80	22.87,51.18	0.23	-4	≤ 26.81	-	0.42
G270-10	8.66283	-2.41668	M3	5000	-1	24.1	7,-	151.37±7.83	135.15,177.55	0.08	-,-	-	-	-
G270-12	8.90835	-10.07196	M2.5	5000	-1	20.3	4,-	41.35±4.11	35.81,45.95	0.06	2,2	15.38±0.59	5.19,5.48	0.62
G218-5	9.56347	+52.33183	K7	5000	-1	25.0	3,-	458.32±25.41	395.96,532.12	0.11	-,-	-	-	-
0093579-3816584	9.89943	-38.28302	M1.8	40	7.7	26.3	2,-	933.87±40.49	703.45,1164.32	0.25	2,-	148.29±24.72	74.29,222.31	0.50
NLTT2196	10.10980	-0.14482	M2.5	5000	-1	24.0	5,-	44.31±5.59	28.74,75.46	0.23	2,3	22.44±0.77	3.92,13.19	0.70
G267-156	10.37616	-33.62605	M0	5000	-5	19.9	2,-	146.85±11.49	132.94,160.78	0.09	-,-	-	-	-
LP193-564	12.24291	+44.58560	M3	100	17.1	21.6	2,-	354.59±25.87	299.39,409.78	0.16	-,-	-	-	-
GJ48	15.64510	+71.67907	M3	5000	-1	8.2	2,-	41.97±3.09	35.71,48.23	0.15	1,1	5.85±1.28	4.59,6.12	0.14
01024375-6235344	15.66502	+62.34522	M1.5	5000	-1	10.0	2,-	181.56±8.34	162.58,200.55	0.10	-,-	-	-	-
G154	17.59742	-67.44385	M2	5000	-1	8.2	2,-	42.44±2.76	40.25,44.63	0.18	-3	≤ 32.49	3.90,7.28	0.33
YZ Cet	18.13012	-16.99774	M4.9	5000	-1	3.7	2,-	6.38±0.49	5.56,7.19	0.10	-,-	-	-	-
GJ1033	18.35040	-22.90210	M4	5000	-1	21.8	2,-	75.43±11.13	68.05,82.79	0.13	-,-	-	-	-
G69-62	19.16491	+25.33127	M0.5	5000	-1	22.5	12,-	441.43±7.31	385.54,504.37	0.05	3,6	24.47±1.50	7.37,30.09	0.03
LHS6027	19.46035	+28.67011	M0.5	5000	-1	24.5	9,-	53.03±5.13	32.65,78.75	0.15	-4	≤ 33.84	20.40,24.06	0.14
LHS1229	19.66840	-0.87490	K7	5000	-9	24.9	-2	≤ 168.67	-	0.31	-,-	-	-	-
01224511-6318446	20.68837	-63.31245	M3.3	40	7.7	28.7	2,-	309.62±37.39	307.15,312.10	0.01	-,-	-	-	-
HD9517	22.90279	-64.61009	M2	5000	-1	17.5	2,-	303.27±16.20	289.50,317.06	0.05	-,-	-	-	-
LHS142	23.10794	-21.90685	M1.3	5000	-9	17.7	2,-	85.01±11.09	73.50,96.52	0.14	-2	≤ 22.95	-	0.22
G272-43	23.49174	-17.64022	M3.5	5000	-1	17.7	2,-	149.44±11.65	74.66,224.22	0.50	1,1	39.11±6.58	18.64,59.59	0.52
UV Cet	24.76279	-17.94948	M5.5	5000	-2	1.7	12,-	7.73±0.04	4.82,13.14	0.15	-,-	5.84±0.04	1.61,41.91	0.17
LHS1289	25.81777	+27.84203	M0.5	5000	-1	20.8	4,-	285.44±12.05	254.09,315.74	0.03	-4	≤ 34.47	-	0.03
LHS6033	26.65419	-8.64973	M4	5000	-1	14.9	3,-	13.43±2.82	9.21,20.51	0.13	-2	≤ 7.43	-	0.58
01505688-5844032	27.73759	-58.73430	M2.9	40	7.7	28.3	2,-	334.03±31.21	313.71,354.31	0.06	1,1	83.78±13.77	77.29,90.26	0.08
GJ3119	27.76794	-6.11851	M5.1	5000	-9	10.0	2,-	13.76±1.94	8.99,18.53	0.35	-,-	-	-	-
NSV15399	28.20667	-22.43486	M0.2	5000	-1	11.1	3,-	406.21±8.45	354.88,454.61	0.11	2,1	31.17±3.60	16.94,41.40	0.18
G272-115	28.29787	-11.09521	M2	5000	-1	20.2	2,-	1615.13±44.68	786.88,2493.37	0.54	2,-	385.63±31.78	167.54,603.74	0.57
02001277-0840516	30.05346	-8.68122	M2	40	7.7	25.4	3,-	543.55±19.23	496.32,568.39	0.00	3,-	132.49±14.03	111.94,150.90	0.12
TZ Ari	30.05618	+13.04850	M4.5	5000	-1	4.5	3,-	10.12±0.68	9.53,10.97	0.03	2,1	1.23,3.31	-	0.07
GJ3125	30.47691	+73.54200	M4.5	5000	-1	11.7	-,-	228.20±17.26	218.99,237.43	0.04	-2	≤ 8.76	-	0.10
LHS1343	31.73910	+45.18358	M0	5000	-1	19.5	2,-	198.65±1.42	120.43,787.07	0.08	-2	≤ 36.37	-	0.33
WW Ari	32.05217	+15.14568	M4.5	5000	-1	19.9	36,-	226.34±3.33	204.83,242.35	0.02	4,-	74.94±7.64	54.49,122.80	0.08
GJ3136	32.22412	+49.44847	M2.9	100	15.1	13.7	5,-	15.29±4.11	14.67,15.89	0.02	4,-	49.29±6.34	30.50,75.19	0.26
G35-32	32.92100	+18.56094	M3	5000	-1	17.5	2,-	23.63±1.44	16.07,34.29	0.04	-2	≤ 14.82	-	0.12
GJ3142	33.22851	+0.00472	M4.1	5000	-1	11.6	5,-	318.74±14.85	308.21,330.00	0.18	4,1	10.04±0.95	6.57,13.77	0.23
02125819-5851182	33.24250	-58.85506	M3.5	40	7.7	21.0	4,-	7.78±0.34	3.52,16.93	0.02	4,-	63.99,108.62	1.43,7.59	0.16
LHS1363	33.55307	-3.96231	M6.5	5000	-1	13.9	22,-	7.93±1.68	6.59,9.27	0.23	15,7	3.70±0.19	-	0.19
GJ3147	34.29271	+35.44205	M5	5000	-1	10.4	2,-	7.93±1.68	6.59,9.27	0.17	-,-	-	-	-
NLTT7704	35.09276	-8.14078	M4.5	5000	-1	24.7	3,-	56.42±9.18	34.35,73.76	0.21	1,2	56.12±1.35	0.00,0.00	0.06
GJ3151	35.10602	+37.79172	M2.5	5000	-1	23.2	2,-	53.24±10.56	52.32,54.15	0.02	-2	≤ 33.60	-	0.04
0220139-5823411	35.21451	-58.39478	M3.2	40	7.7	27.8	4,-	303.29±22.20	195.30,400.02	0.26	1,3	102.79±10.20	75.74,111.60	0.19
G173-53	35.56164	+47.88010	M0.5	5000	-1	11.9	2,-	209.50±10.36	202.88,216.11	0.03	-,-	-	-	-
02242453-7033211	36.10342	-70.55590	M4	40	7.7	28.3	7,-	121.61±10.41	78.81,181.96	0.18	-4	≤ 60.82	-	0.34
G35-43	36.23760	+25.55099	M3.5	5000	-1	23.8	-,-	14.78±4.76	14.00,15.54	0.05	-2	≤ 55.72	-	0.07
LHS1408	37.13411	-20.04025	M2.9	5000	-1	18.9	2,-	82.83±17.13	36.57,59.40	0.13	-2	≤ 26.77	-	0.37
GJ102	38.40501	+24.92627	M4	5000	-1	9.8	4,-	20.50±2.60	18.83,26.77	0.05	-2	≤ 14.61±2.12	10.41,20.36	0.13
EX Cet	39.06754	-6.87480	M4.3	40	7.7	29.4	2,-	82.83±17.13	78.83,86.87	0.05	1,1	42.20±9.93	39.59,44.86	0.06
LHS1408	39.06754	-6.87480	M4.3	40	7.7	29.4	2,-	82.83±17.13	78.83,86.87	0.05	1,1	42.20±9.93	39.59,44.86	0.06
GSC8056-0482	39.21581	-52.05106	M3	5000	-1	7.3	-,-	1007.19±36.60	1002.81,1011.63	0.00	-2	≤ 6.00	127.00,156.06	0.10
LHS1427	39.44249	-7.09771	M4.5	5000	-1	21.1	4,-	23.36±2.73	13.27,35.57	0.21	2,2	10.20±0.58	4.90,8.46	0.24
LHS157	39.96241	-34.13532	M2.5	5000	-1	15.6	7,-	12.60±1.06	9.83,15.94	0.05	-,-	≤ 5.27	-	0.23
G75-35	40.31364	-4.53836	M4	5000	-1	12.5	2,-	42.28±5.80	33.56,51.00	0.21	-,-	18.13±3.82	13.09,23.16	0.28

TABLE 1—Continued

Name ^a	RA J2007 (deg)	DEC J2007 (deg)	SpT	Age ^b (Myr)	Ref	Dist. (pc)	NUV det ^c , u.l.d	NUV μ^e (μ Jy)	NUV Min,Max ^g (μ Jy)	NUV MAD ref ^h	FUV det ^c , u.l.d	FUV μ^e (μ Jy)	FUV Min,Max ^g (μ Jy)	FUV MAD ref ^h
VX Ari	41.06648	+25.52266	M3	5000	-1	7.6	2-	15.28±2.00	13.82±16.74	0.10	-2	< 4.10	-	0.04
LTT1339	41.29472	-43.74293	M5	5000	-1	10.6	2-	23.66±2.92	21.88±25.44	0.08	-2	< 12.23	-	0.10
LP993-116	41.30963	-43.73617	M4	5000	-1	7.0	2-	30.56±1.92	29.93±1.18	0.07	2-	13.44±1.89	10.25,16.64	0.24
02543316-5108313	43.63845	-51.14208	M1.4	40	7.7	2.3	2-	572.88±33.97	530.42±615.31	0.02	2-	142.10±28.74	123.72,160.46	0.13
LP591-156	44.01666	-0.60908	M5	5000	-1	23.4	3-	68.88±4.08	43.48±11.57	0.05	2,2	31.30±2.10	18.84,40.30	0.18
C75-55	44.58369	-0.99318	M0.5	5000	-1	24.4	7-	236.29±5.19	115.76,267.79	0.04	5,2	22.40±2.10	6.01,32.92	0.42
LHS1483	44.79537	+36.61067	M3.5	5000	-1	21.6	2-	12.31±3.79	10.73,13.90	0.13	-2	< 22.82	-	0.04
LP771-72	45.65937	-18.16601	M2.5	5000	-1	20.9	4-	96.70±4.43	71.24,129.60	0.09	4,4	23.86±1.29	8.95,21.05	0.45
C77-24	46.88410	-6.61386	M:	5000	-1	16.5	1,1	4.62±0.84	3.24,6.02	0.30	1,1	3.86±0.63	0.00,0.00	0.03
NLT79942	46.94557	+24.96519	M4.5	5000	-1	20.7	2-	60.02±1.31	31.62,88.40	0.47	1,1	33.84±6.58	30.59,37.11	0.10
LP831-45	48.57626	-23.15794	M3.5	5000	-5	15.4	2-	36.62±1.88	25.38,49.45	0.17	14,2	13.23±0.92	4.20,25.26	0.32
LTT1540	48.68641	-26.44605	K7	5000	-5	18.4	2-	1090.88±30.97	1058.61,1123.14	0.03	1,1	29.01±5.57	0.00,0.00	0.13
C78-24	48.68751	+48.51905	M1	5000	-1	17.8	4-	83.55±14.96	69.24,97.90	0.17	-2	< 47.27	-	0.11
C77-46	50.44616	-6.67347	M2	5000	-1	17.7	4-	116.53±7.30	91.76,127.04	0.02	1,3	45.97±0.86	0.00,0.00	0.10
03244056-3904227	51.16925	-39.07303	M4.1	40	7.7	21.7	2-	474.29±23.10	210.49,738.12	0.56	2-	116.12±18.02	52.83,179.41	0.54
NSV1166	52.33260	-11.67896	K7	5000	-1	21.7	3-	639.84±17.41	594.55,678.41	0.05	2,1	66.83±8.23	29.95,98.60	0.37
03315564-4359135	52.98214	-43.98709	M0	40	7.7	28.4	4-	1405.60±28.24	1270.33,1506.82	0.03	2-	189.00±32.08	156.96,221.08	0.17
LHS1572	54.54335	-68.94513	M2.5	5000	-1	15.8	2-	21.97±5.06	15.03,28.91	0.32	-3	< 19.91	-	0.15
C6-28	55.93885	+16.66663	M1	5000	-1	16.3	4-	125.83±8.52	75.64,154.07	0.11	1,2	< 23.82	-	0.04
HD23453	56.58475	+26.21510	M0	5000	-1	14.6	3-	362.86±1.52	339.29,396.41	0.04	1,2	28.36±1.07	0.00,0.00	0.04
C80-21	56.84763	-1.97274	M2.8	100	15.1	16.3	2-	364.93±15.73	351.56,378.32	0.04	-2	< 2.38	-	0.44
LHS183	57.68379	-6.09711	M3.5	5000	-1	9.5	2-	7.31±1.33	5.46,9.17	0.25	-2	< 2.38	-	0.44
CJ3252	57.75023	-0.88016	M6	5000	-1	14.7	2-	12.50±3.95	10.98,14.02	0.12	-2	< 66.89	-	0.55
CJ3256	58.09746	-22.88212	M2	5000	-1	23.8	3-	63.03,107.57	36.03,107.57	0.14	-2	35.93±8.95	33.64,38.19	0.06
HIP18115	58.60663	-9.15868	M3	5000	-1	17.3	2-	145.01±11.86	123.04,167.00	0.15	2-	< 36.57	-	0.18
LHS1616	59.37471	+26.08952	M3	5000	-1	19.7	2-	35.90±8.60	23.52,48.28	0.34	-2	25.27±1.35	0.00,0.00	0.34
LHS1628	61.64528	-20.85464	K7	5000	-1	23.6	3-	850.85±18.88	801.19,889.97	0.03	1,2	67.33±3.88	8.60,105.94	0.85
LHS5094	66.63590	-30.80127	M4.5	5000	-1,1	11.0	2-	227.55±9.28	54.90,400.20	0.76	1,1	< 28.82	-	0.15
LHS1672	67.14865	-25.17006	M2.5	5000	-1	19.2	2-	43.88±9.36	22.75,65.03	0.48	-2	< 28.82	-	0.15
NLTT13422	67.71682	-8.82240	M4	5000	-1	19.6	2-	22.75,65.03	22.75,65.03	-	-2	< 32.83	-	0.11
CDDM104367-2722B	69.16540	-27.36866	M:	5000	-2	21.1	2-	33.85±10.95	20.21,47.50	0.40	-3	31.70	-	0.17
CDDM104367-2722A	69.16965	-27.35540	M:	5000	-2	21.2	2-	36.35±8.33	26.07,46.65	0.28	-3	34.10	-	0.13
04365738-1613065	69.23921	-16.21856	M3	40	7.7	22.9	3-	577.83±26.34	424.61,789.50	0.18	3-	184.24±23.48	120.46,279.77	0.21
LTT2050	69.42400	-11.03925	M2	5000	-9	11.1	2-	48.61±3.95	41.51,55.72	0.15	-2	< 10.84	-	0.10
LP655-43	69.51041	-5.93736	M4	5000	-1	14.7	6-	62.36±4.74	26.43,149.34	0.34	1,3	30.12±3.54	23.47,38.10	0.16
LP655-48	70.09733	-5.50212	M6	90	13.1	10.3	2-	17.04±3.14	15.28,18.81	0.10	-2	< 14.25	-	0.20
C8-52	70.09733	-5.50212	M6	90	13.1	10.3	2-	88.44±10.72	70.83,113.51	0.17	-2	< 41.57	-	0.08
GJ1176	70.73375	+20.77621	M1.5	5000	-1	24.5	5-	90.73±4.36	74.47,106.99	0.18	-2	< 75.03	-	0.10
NLTT13837	71.03374	+18.95600	M2	5000	-1	9.3	2-	119.49±10.43	104.55,132.67	0.08	-4	151.20±13.61	65.20,188.40	0.07
NLTT14116	73.10194	+14.02270	M4.3	300	13.1	19.4	4-	594.45±15.56	471.60,721.91	0.10	4-	< 12.99	-	0.24
LHS1712	73.45825	-16.82318	M3.3	100	15.1	16.3	4-	45.00±5.78	34.58,62.83	0.08	-3	< 35.43	-	0.27
C85-36	73.51506	-17.77342	M2.1	5000	-9	12.4	3-	94.41±9.65	58.99,109.85	0.04	-3	< 8.46	-	0.04
CJ3325	75.31506	+24.87273	M2	5000	-1	19.0	4-	9.95±2.49	5.78,14.19	0.41	-4	< 8.46	-	0.27
LHS28	75.83323	-17.37441	M3.2	5000	-9	9.2	3-	113.04±1.44	104.72,119.44	0.06	-2	< 8.90	-	0.65
CJ3335	75.85381	+53.12548	M0	5000	-1	14.0	5-	235.12±21.85	230.88,239.35	0.02	1,1	177.09±17.68	0.00,0.00	0.54
LHS1748	77.29183	+15.45780	M3.5	300	13.1	21.7	2-	45.01±6.26	32.99,57.02	0.27	-2	< 17.80	-	0.11
C85-52	78.17652	-19.66613	M2	5000	-1	21.6	2-	71.99±13.96	32.71,111.27	0.55	-2	< 30.97	-	0.05
LHS1749	79.00153	-31.29600	M2.5	5000	-1	17.9	3-	3844.76±39.70	3804.04,3920.06	0.00	-2	< 30.97	-	0.05
LHS1767	82.76870	-30.19654	M3.5	5000	-2	18.7	2-	8.06±2.01	7.66,8.46	0.05	-2	< 30.97	-	0.05
CJ1083A	85.10734	+24.80177	M5.5	5000	-1	10.4	2-	19.50±4.13	19.22,19.77	0.01	-2	< 30.97	-	0.05
LTT2396	88.25118	-5.99552	M0	5000	-1	20.1	4-	540.53±34.55	398.23,759.70	0.11	-2	< 30.97	-	0.05
LHS1805	90.29606	+59.59519	M3.7	5000	-9	7.9	3-	5.86±1.01	3.65,7.95	0.33	-2	< 19.71	-	0.04
LHS215	92.58342	+82.10416	M2	5000	-1	9.4	2-	31.56±2.88	30.60,32.53	0.03	1,1	5.07±1.11	4.82,5.31	0.05
CJ3391	95.30456	-44.24139	M2	5000	-1	23.1	1,1	348.94±18.90	263.71,434.20	0.24	2-	87.55±18.97	82.44,92.69	0.06
LHS1804	95.47286	-22.72821	M1	5000	-1	24.7	2-	394.98±36.13	382.47,407.54	0.03	-2	< 59.38	-	0.38
LP160-22	95.96342	+45.66750	M5	5000	-1	16.4	2-	23.48±6.35	16.11,30.85	0.31	-2	< 59.38	-	0.38
0633437-7537482	95.96342	+45.66750	M2	5000	-1	8.7	3-	36.26±2.51	30.68,43.95	0.01	3-	8.70±1.80	6.68,11.84	0.12
66334690-7537301	98.42814	-75.62945	M2	5000	-1	8.7	3-	7.30±1.93	7.21,7.40	0.01	-3	< 6.67	-	0.05
CD-6114439	98.44292	-75.62465	M3	5000	-1	9.0	2-	1873.73±93.37	1333.12,1440.08	0.03	3-	121.35±16.85	88.06,144.65	0.10
LHS1864	99.95833	+51.47805	K7	1000	15.1	21.9	3-	373.73±5.58	72.78,103.64	0.03	1,2	30.42±5.10	21.74,46.29	0.06
LHS1867	100.95736	+61.13746	M2.5	5000	-2	19.1	3-	92.34±9.33	72.78,103.64	0.03	-2	< 45.41	-	0.05
LHS1867	101.53020	+32.55433	M0.9	5000	-9	25.0	-2	71.98±8.04	70.07,73.89	0.03	-2	16.84±4.52	14.72,18.98	0.13
CJ3423	105.84638	+34.69777	M4	5000	-1	12.0	2-				-2			

TABLE 1—Continued

Name ^a	RA J2007 (deg)	DEC J2007 (deg)	SpT	Age ^b (Myr)	Ref	Dist. (pc)	NUV det ^c , n.i.d	NUV μ^e (μ Jy)	NUV Min,Max ^g (μ Jy)	NUV MAD rel ^f	FUV det ^c , n.i.d	FUV μ^e (μ Jy)	FUV Min,Max ^g (μ Jy)	FUV MAD rel ^g
G250-34	106.95868	+67.20122	M1	5000	-1	17.7	3-	80.81±6.12	59.24,97.50	0.03	-3	≤ 12.98	0.18	
G107-61	109.53356	+39.27459	M0	5000	-1	14.5	3-	101.30,108.85	101.30,108.85	0.04	-3	≤ 13.18	0.01	
BD-201790	110.93162	+20.41628	K7	1000	15.1	25.8	2-	3318.81,3425.72	3318.81,3425.72	0.02	2-	255.47,351.52	0.16	
BD+051668	111.85320	+5.21861	M3.5	5000	-1	3.8	3-	4.54,4.92	4.54,4.92	0.01	2.1	1.10,1.29	0.01	
G111-5	112.45149	+41.22417	M4.5	5000	-1	10.0	2-	7.50±1.84	3.36,11.65	0.55	3-	-	-	
BL Lyn	112.98827	+36.22933	M3.3	300	13.14	11.8	3-	144.11±5.37	137.40,153.46	0.03	3-	24.17,42.47	0.02	
GJ3454	114.10517	+7.07806	M5	5000	-2	8.6	-	-	137.40,153.46	-	2-	11.40,15.26	0.14	
NLTT18210	114.54010	-31.20493	M2.5	5000	-1	16.5	2-	22.68±7.39	18.32,27.03	0.19	-	-	-	
LHS1937	115.27804	+17.64514	M6.5	5000	-1	23.0	2-	22.68±5.76	16.83,28.34	0.26	-2	≤ 14.41	0.49	
LP423-31	118.09996	+16.20367	M7	100	13.1	12.3	2-	22.33±1.89	10.68,49.31	0.34	2.5	8.44,27.82	0.17	
GJ3478	121.49380	+26.28133	K7	5000	-1	17.9	2-	371.85±17.99	362.77,380.90	0.02	1.1	0.00,0.00	0.05	
G111-56	121.92982	+42.29207	M4.5	5000	-1	17.6	2-	27.43±6.02	17.19,37.67	0.37	1.1	0.00,0.00	0.53	
GJ2066	124.03253	+1.30269	M2.2	5000	-1	9.1	4-	35.29±2.23	30.31,42.33	0.08	-4	≤ 6.08	0.09	
LHS2025	127.87952	+73.06329	M4	5000	-8	12.2	10-	3.70±0.44	1.73,7.99	0.38	-4	-	0.59	
LHS6149	128.60825	+1.14503	M3.5	5000	-1	19.7	2-	7.32±1.94	7.22,7.41	0.01	-2	≤ 4.93	0.08	
LHS2029	129.28293	+15.12757	M2.5	5000	-1	16.1	2-	28.97±6.22	25.35,32.58	0.12	-2	≤ 77.92	0.73	
G114-10	129.72672	-9.56664	M2	5000	-16	20.5	5-	63.82±6.42	51.40,77.91	0.05	-3	≤ 81.88	0.03	
G114-14	130.59660	-4.89911	M2.5	5000	-1	23.7	3-	16.15±2.72	12.08,19.38	0.14	-	-	-	
LHS2063	133.16916	+28.31590	M4.1	5000	-1	13.0	-	-	12.08,19.38	-	-	-	-	
NLTT20426	133.18605	+22.51426	M3.5	5000	-1	24.1	2-	344.12±20.18	268.68,419.52	0.22	2-	≤ 21.12	0.02	
G41-8	134.08146	+12.66344	M4.5	5000	-1	11.6	8-	16.85±1.14	9.93,25.11	0.29	2-	84.68±13.06	0.22	
LHS2078	134.66045	+20.54641	M0	5000	-1	20.6	17-	1121.28±4.68	1002.08,1212.74	0.03	4.4	4.66,7.25	0.41	
G41-14	134.73540	+8.47328	M3.5	5000	-1	6.8	6-	216.99±2.29	107.90,504.39	0.22	6-	7.30,20.03	0.29	
LHS2090	135.09723	+21.83369	M6.5	5000	-1	6.3	4.1	2.63±0.18	1.28,5.68	0.14	3.2	37.43,132.76	0.23	
GJ1119	135.13424	+46.58557	M4.5	5000	-1	10.3	3-	18.03±1.98	13.74,20.91	0.08	-	0.57,3.12	0.50	
LHS6167	138.90101	-10.59677	M5	5000	-1	6.7	19-	13.92±0.23	7.03,26.24	0.27	4.2	-	-	
G47-33	139.69222	+26.75246	M1.5	5000	-1	19.6	4-	129.50±9.32	85.63,149.25	0.05	1.3	2.36,8.37	0.36	
GJ3554	140.45383	+43.50768	M4	5000	-1	14.5	2.1	32.29±1.44	11.40,43.50	0.04	-	22.40,25.43	0.17	
G115-72	140.71468	+46.78336	M1.5	5000	-1	22.5	2-	244.23±18.53	242.04,246.39	0.01	1.1	-	-	
LP211-12	142.50725	+39.62293	M2.5	5000	-1	19.2	2-	24.01±4.60	22.71,25.29	0.05	-	25.62,55.99	0.37	
LHS2149	142.68465	-0.32158	M3.5	5000	-1	9.7	-	-	22.71,25.29	-	2.4	3.29±0.07	0.27	
GJ353	142.98422	+36.31921	M0.6	5000	-9	13.5	3-	123.01±6.26	113.72,138.09	0.03	2-	1.07,1.59	0.09	
GJ362	145.71175	+70.03890	M3	5000	-1	11.5	4-	119.28±3.27	104.19,142.14	0.05	4-	13.83,16.71	0.16	
LHS273	146.19386	-18.21393	M3.8	5000	-9	11.0	3-	28.71±2.79	22.48,31.98	0.01	-3	19.74,32.48	0.12	
NLTT22440	146.28466	+71.74734	M5	5000	-1	14.3	2-	15.73±3.63	14.74,16.73	0.06	-2	≤ 8.50	0.14	
LHS2188	146.70273	+76.04198	M1.5	5000	-1	15.9	2-	80.95±5.08	79.43,82.47	0.02	-	-	-	
LP728-70	147.66923	-13.81092	M4	5000	-1	15.3	-	-	79.43,82.47	-	-2	≤ 18.11	0.43	
LP788-49	147.84814	-17.73986	M2	5000	-1	20.4	2-	56.34±10.25	36.62,76.03	0.35	-	-	0.01	
GJ3571	148.47943	+20.94692	M4.5	5000	-1	9.2	2-	15.13±2.57	9.48,20.77	0.37	-2	-	0.22	
GJ3572	148.93162	+35.36111	M3	5000	-1	20.1	7-	117.70±5.08	85.73,152.35	0.11	4-	≤ 4.61	0.12	
G1373	149.03483	+62.78733	M0	5000	-1	10.5	6-	349.41±2.22	313.71,365.08	0.01	-	31.51,47.59	0.03	
NLTT23164	150.52396	+69.75774	M4.5	5000	-1	19.4	5-	4.03±0.74	2.82,6.06	0.19	-4	≤ 5.81	0.43	
G43-23	150.67726	+14.98639	M4	5000	-1	17.1	2-	11.06±3.25	4.65,17.46	0.58	-2	≤ 10.72	0.80	
LHS2220	151.68188	+41.71382	M0.5	5000	-1	22.2	2-	100.64±9.11	97.29,103.99	0.03	-	10.26±1.82	0.25	
G162-25	153.07333	-3.74614	M1.9	5000	-9	7.8	2-	116.75,120.35	116.75,120.35	0.02	2-	-	-	
NLTT24199	155.96649	+43.89254	M4.5	5000	-1	19.8	4-	41.23±5.08	20.54,61.63	0.36	-	11.85±3.58	0.19	
LHS2259	156.29380	-10.22846	M3.5	5000	-9	12.5	4-	141.53±5.63	128.38,170.92	0.03	2-	≤ 26.11	0.13	
LHS2260	156.37576	+26.38752	M3.5	5000	-1	17.5	5-	25.43±4.71	12.07,46.89	0.53	-4	5.49±0.61	0.04	
BD+012447	157.23029	+0.83959	M2.2	100	15.9	7.2	4-	45.14±0.89	40.40,50.71	0.08	3-	4.92,6.45	0.05	
LHS283	158.85442	+69.44861	M3.5	5000	-1	13.2	-	-	40.40,50.71	-	-2	≤ 11.60	0.15	
G196-37	159.20144	+50.91737	M4.5	5000	-1	20.0	2-	80.66±12.05	58.68,102.64	0.27	1.1	9.59,14.11	0.19	
NLTT24892	159.47988	+12.77695	M2.5	5000	-1	21.7	5-	26.89±3.81	16.95,44.22	0.29	1.2	0.00,0.00	0.05	
LHS2295	159.91762	-6.92397	M2.5	5000	-1	16.8	2-	53.90±7.78	53.34,54.44	0.01	-2	16.21±0.73	0.51	
LHS2317	162.60849	+33.10022	M4	5000	-1	22.9	3-	17.11±3.72	11.01,26.85	0.19	-3	≤ 19.57	0.06	
WofR58	162.71512	+8.80652	M3.9	5000	-9	6.8	13-	7.91±0.34	4.48,12.18	0.21	1.4	≤ 16.63	0.59	
LHS2334	164.40520	+69.59672	K7	5000	-1	23.0	2-	420.82±15.71	407.86,433.83	0.03	1.1	0.74,6.57	0.67	
G408	165.01684	+22.83241	M3	5000	-6	6.7	2-	21.11±23.57	21.11,23.57	0.06	1.1	25.18±2.04	0.24	
HD95650	165.66006	+21.96704	M0	3000	-1	16.0	2-	451.87±11.22	448.57,455.16	0.01	2-	0.00,0.00	0.34	
G56-11	165.78440	+15.29757	M4	5000	-1	14.1	2-	52.56±4.01	55.94,62.98	0.03	2-	33.85,68.75	0.39	
NLTT26114	165.83817	+13.63266	M3	300	13.1	14.1	2-	60.61±0.64	44.65,60.48	0.15	-	15.00,17.18	0.07	
G412B	166.36894	+43.52326	M6	5000	-1	4.9	2-	10.87±0.64	10.36,10.98	0.03	-	-	-	
G163-51	167.02714	-5.23062	M3	5000	-2	23.1	6-	42.48±6.43	19.64,75.77	0.39	-3	≤ 42.54	0.13	

TABLE 1—Continued

Name ^a	RA J2007 (deg)	DEC J2007 (deg)	Spt	Age ^b (Myr)	Ref	Dist. (pc)	NUV det ^c , u.l.d	NUV μ^e (μ Jy)	NUV Min,Max ^g (μ Jy)	NUV MAD rel ^f	FUV det ^c , u.l.d	FUV μ^e (μ Jy)	FUV Min,Max ^g (μ Jy)	FUV MAD rel ^f
LP214-42	167.20536	+39.91998	M5	5000	-1	19.1	-	-	19.64,75.77	-	-2	-	-	0.07
G163-53	167.30035	-4.60716	M0.5	5000	-1	25.1	171.94±15.79	-	150.64,186.42	0.04	-2	-	-	0.06
LHS2367	167.77289	+30.44563	K7	5000	-1	11.9	676.64±16.32	-	632.84,720.44	0.03	-2	-	12.65,24.97	0.33
CW UMa	167.96518	+33.53671	M3.5	300	13.1	13.6	247.49±9.95	-	239.26,255.71	0.06	2-	50.27,52.27	0.02	0.02
G11200.1-102518 ^h	168.25272	+10.41805	M3	300	13.1	23.0	134.53±14.97	-	113.10,155.95	0.16	-2	-	-	0.06
G122-8	168.86102	+41.08741	M3	5000	-1	23.7	27.29±7.09	-	20.89,33.70	0.23	-2	-	-	0.82
LP792-17	170.24922	-17.03051	M2.5	5000	-1	21.4	31.79±8.42	-	28.62,34.94	0.10	-2	-	-	0.08
LHS2403	171.25079	+43.32725	M5	5000	-1	17.1	39.70±6.15	-	30.59,48.80	0.23	1,1	-	16.90,20.88	0.11
LP792-33	173.07950	-16.96916	M1.5	5000	-1	22.9	145.03±17.33	-	137.45,152.60	0.05	-2	-	-	0.07
LHS2427	173.65689	-23.87146	M0	5000	-1	17.7	54.95±6.47	-	44.58,65.45	0.19	-2	-	-	-
G197-21	174.41126	+70.03291	M4	5000	-1	24.4	43.09±4.30	-	41.56,44.65	0.04	-2	-	-	-
GJ3684	176.77071	+7.86920	M4	5000	-6	5.4	179.31±10.37	-	118.64,239.99	0.34	-2	-	-	-
GJ445	176.92978	+78.69210	M4	5000	-6	5.4	1.07±0.09	-	0.64,1.57	-	-2	-	-	-
LHS2460	177.07950	+0.80220	M4.5	5000	-1	3.4	32.73±6.63	-	22.56,38.56	0.04	3,1	0.14,0.46	0.43	0.02
G10-52	177.14814	-11.28743	M3	5000	-1	20.0	145.02±14.55	-	121.09,168.91	0.16	-2	-	-	0.16
G1450	177.77992	+35.27251	M1	5000	-1	8.6	77.29±3.71	-	76.35,78.23	0.01	1,1	6.30,7.62	0.09	0.14
NLTT29087	179.47241	-23.81696	M4.5	5000	-1	21.0	87.35±7.74	-	51.24,153.51	0.31	1,2	34.62,47.45	0.14	0.14
LP754-30	180.57404	+28.58721	M2.5	5000	-1	20.2	73.82±6.70	-	68.84,78.71	0.07	1,1	0.00,0.00	0.06	0.23
LHS2516	182.19560	-10.26717	M3	5000	-1	22.7	39.95±10.39	-	36.95,42.92	0.07	-2	-	-	0.12
LHS2520	182.27922	+47.60089	M4	5000	-1	22.5	6.96±0.87	-	5.26,8.25	0.19	1,5	0.00,0.00	0.12	0.12
LHS2519	182.52319	-15.07240	M3.8	5000	-9	8.9	11.16±1.75	-	3.15,19.16	0.72	-2	-	-	-
LP734-34	182.61857	-13.17386	M4	5000	-1	12.9	66.87±5.85	-	63.95,69.79	0.04	-2	-	-	0.24
LP794-30	182.79855	-19.96093	M3	5000	-1	12.8	15.76±2.74	-	11.24,24.89	0.16	-2	-	-	0.05
G197-49	183.08769	+54.48593	M0	5000	-1	15.3	318.30±8.33	-	298.37,337.89	0.06	-2	-	8.74,10.88	0.10
GJ1154	183.56705	+0.62344	M5	5000	-1	8.4	33.31±1.29	-	22.60,41.85	0.15	3-	7.70±1.49	0.06	0.06
GJ1156	184.74498	+11.12647	M5	5000	-1	6.5	20.62±0.72	-	14.94,30.59	0.11	2-	-	-	-
G148-43	184.77429	+31.84539	M3	5000	-1	16.6	58.35±3.72	-	49.68,66.74	0.14	-2	-	-	-
LHS2544	185.44641	+28.38251	M0	5000	-1	24.7	416.93±13.08	-	379.17,456.04	0.09	-2	-	-	-
G237-61	185.44641	+68.26814	M4	5000	-1	23.3	21.21±3.17	-	20.47,21.99	0.04	-2	-	-	-
G13-33	185.71034	-4.07966	M4.5	5000	-1	21.3	154.87±14.55	-	141.51,168.23	0.07	-2	-	47.46,63.74	0.15
G13-39	186.93575	-3.25024	M3.5	5000	-1	15.0	109.82±5.14	-	12.38,19.21	0.09	-6	-	-	-
GJ3729	187.26157	+41.73004	M3.5	300	13.1	16.2	4.93±0.209	-	4.28,19.21	0.07	-2	-	-	-
Wolf424	188.31902	+9.02144	M5	5000	-2	4.4	29.82±0.39	-	97.58,137.02	0.05	2-	22.86,28.63	0.11	0.37
LP795-38	189.33978	-20.87722	M4	5000	-1	15.3	15.47±4.57	-	20.22,42.23	0.22	6-	5.85,13.37	0.21	0.21
LHS2613	190.70677	+41.89645	M4	5000	-8	10.6	75.13±3.61	-	15.29,15.66	0.01	-2	-	-	-
LHS2526	191.00222	-11.17535	M4.5	5000	-1	12.5	44.17±2.64	-	12.56,15.88	0.37	-2	-	-	-
LHS2634	191.78974	-3.57160	M3.5	5000	-2	19.4	38.70±2.43	-	31.43,59.62	0.06	-4	-	-	-
G14-6	192.68147	-0.76890	K7	5000	-9	10.8	549.52±7.85	-	511.98,568.72	0.00	3-	27.22,57.14	0.35	0.35
LP854-3	194.05512	-22.08333	M2.5	5000	-1	23.2	33.50±7.13	-	20.67,42.20	0.12	-2	-	-	0.62
NSV6039	194.41333	+35.22178	M4	300	13.1	18.1	357.87±16.12	-	177.24,538.53	0.50	2-	74.77±12.46	0.01	0.01
BF CVn	194.41712	+35.22465	M0.5	150	13.1	18.1	989.57±26.09	-	977.36,1001.77	0.01	2-	190.68±19.64	0.00	0.00
LHS231	194.82633	-0.17695	M4	5000	-1	17.5	46.52±12.47	-	40.61,52.43	0.13	1,1	0.00,0.00	0.86	0.86
G14-18	195.01591	-5.62986	M3	5000	-1	17.2	39.86±3.07	-	32.99,53.34	0.11	2,2	6.06,10.47	0.35	0.35
GJ493.1	195.13778	+5.68600	M4.5	5000	-1	8.1	92.99±3.04	-	73.04,125.00	0.10	-2	-	-	-
G14-34	197.21273	-1.51876	M3	5000	-1	21.2	33.64±4.07	-	15.69,52.81	0.16	-6	-	-	0.18
GJ1167A	197.39546	+28.98506	M4.8	300	13.13	12.4	62.82±1.08	-	14.08,271.77	0.32	8-	6.00,458.07	0.08	0.08
LHS2686	197.55101	+47.75408	M5	5000	-8	11.0	45.16±3.60	-	22.32,68.00	0.51	1,1	10.19,14.71	0.18	0.18
LHS2695	198.26868	+20.19097	M3.5	5000	-1	17.5	23.19±5.84	-	9.46,36.90	0.59	-2	-	-	0.17
NLTT33417	198.59759	+66.37588	M6	5000	-1	19.1	16.80±4.66	-	4.89,28.71	0.71	-2	-	-	0.04
LP164-62	199.49314	+36.29848	M1	5000	-2	21.6	107.10±12.32	-	99.84,114.35	0.07	-2	-	-	0.04
LHS2724	200.24302	+34.27837	M1	5000	-9	7.9	85.69±4.76	-	68.25,102.36	0.15	-4	-	-	0.29
G1514	202.50134	+10.37508	M1.1	5000	-1	16.1	96.22±4.02	-	95.86,96.58	0.00	-2	-	-	0.14
BPSRS16078-0011	202.94370	+29.27657	M4	5000	-1	12.4	43.50±3.64	-	127.15,148.65	0.08	2-	26.71,35.24	0.14	0.14
NLTT34410	203.16287	+30.98511	M4.5	5000	-4	24.3	173.86±47.21	-	168.92,1758.77	0.05	2-	6.67,11.15	0.25	0.25
G62-64	205.60792	-1.68658	K5	5000	-1	5.4	71.00±2.15	-	67.04,74.96	0.06	-2	-	-	-
NSV6431	206.43598	+14.88869	M2	5000	-1	16.1	50.11±3.19	-	38.88,62.13	0.06	-2	-	-	0.11
G150-46	208.15100	+14.42172	M2	5000	-1	17.9	6.37±1.29	-	4.90,7.85	0.23	-2	-	-	-
LP229-13	209.17163	+43.71646	M6.5	5000	-1	13.8	5.07±0.80	-	3.14,8.17	0.18	-2	-	-	-
LP799-2	209.56690	-12.04969	M4	5000	-1	15.8	19.44±5.45	-	16.43,22.44	0.15	-2	-	-	-
LP739-3	209.58219	-13.27368	M4	5000	-1	8.6	31.56±2.64	-	30.19,32.93	0.04	-2	-	-	-
GJ3820	209.79243	-19.83465	M4	5000	-1	8.6	-	-	-	-	-2	-	-	-

TABLE 1—Continued

Name ^a	RA J2007 (deg)	DEC J2007 (deg)	SpT	Age ^b (Myr)	Ref	Dist. (pc)	NUV det ^c , u.l.d	NUV μ^e (μ Jy)	NUV Min,Max ^g (μ Jy)	NUV MAD rel ^f	FUV det ^c , u.l.d	FUV μ^e (μ Jy)	FUV Min,Max ^g (μ Jy)	FUV MAD rel ^f
LHS2842	210.26169	-2.65370	M1	5000	-1	10.2	2-	103.53±3.69	99.16±10.71	0.04	1,1	6.77±0.48	0.00,0.00	0.14
GJ3822	210.58196	+13.68937	M0.5	5000	-1	19.5	4-	293.42±11.73	278.80,306.14	0.02	1,1	23.75±4.72	22.28,25.21	0.06
LHS2864	211.94767	+57.19627	M:	5000	-1	21.1	2-	38.02±6.67	38.02±6.67	0.24	-	-	-	-
LHS2866	212.09124	+75.85279	M0.5	5000	-1	24.8	3-	55.27±7.02	47.97,64.83	0.10	-	-	-	-
GQ Vir	213.26928	-12.02471	M4.5	5000	-1	10.9	3-	133.05±5.43	69.48,213.49	0.40	2-	13.86±3.24	10.47,17.25	0.24
GJ3839	214.26095	-31.71283	M4	5000	-1	19.2	2-	377.23,698.87	377.23,698.87	0.30	2-	215.53±25.19	105.43,325.66	0.51
LP381-49	215.58323	+23.87649	M5	5000	-1,10	16.1	5-	23.05±2.69	16.56,32.09	0.16	-2	≤ 10.51	-	0.12
LP800-58	216.30493	-16.41551	M5.5	5000	-1	16.3	3-	17.92±4.61	16.49,20.09	0.04	-2	≤ 18.81	-	0.17
LHS373	217.37162	+15.53517	M2.5	5000	-1	14.3	5-	75.84±4.61	70.12,84.21	0.06	-2	≤ 13.82	-	0.15
GJ3856	218.04530	+16.01360	M4	5000	-1	15.6	5-	234.84±7.17	40.20,913.96	0.30	-	≤ 38.21	-	0.11
NTT38526	222.54636	+32.30442	M3	5000	-1	23.8	3-	26.67±6.59	19.26,35.86	0.23	-3	42.53±1.46	11.07,94.13	0.22
G166-49	223.11875	+12.39195	M2	5000	-1	15.0	2-	128.56±1.07	90.06,259.42	0.13	15,1	≤ 52.14	-	0.08
G179-7	225.29941	+35.45370	M1.5	5000	-1	24.8	8-	59.43±4.69	32.54,84.20	0.24	-6	≤ 63.41	-	0.24
LP859-11	227.09715	-23.86074	M1.5	5000	-1	22.9	2-	50.89±5.79	89.41,90.62	0.01	-2	-	-	-
LP222-65	229.16916	+39.18009	M6.5	5000	-1	15.5	1,1	90.02±15.87	8.85,11.68	0.08	-	-	-	-
OT Ser	230.47071	+20.97801	M1	15	13,13	11.4	3-	83.32±14.55	693.96,1008.00	0.06	2-	138.37±10.62	130.39,146.33	0.06
GJ224-65	230.96365	+58.46903	M3.5	5000	-1	19.9	2-	93.91±12.90	78.29,109.54	0.17	1,1	29.76±4.12	0.00,0.00	0.39
LP176-55	233.41384	+46.25113	M3.5	5000	-1	20.3	7-	9.24±1.42	4.66,21.92	0.28	-8	≤ 9.14	-	0.19
LHS1122	237.40814	+34.81675	M4	5000	-1	17.0	3-	65.40±6.44	22.86,134.38	0.41	2,1	35.18±6.39	24.33,53.87	0.11
G256-25	237.47758	+79.66461	M5	5000	-3	13.9	2-	20.99±3.93	18.49,23.49	0.12	1,1	11.47±2.76	9.35,13.60	0.18
LHS3129	238.27654	+34.75386	M2.5	5000	-1	19.2	2-	46.20±8.89	45.75,46.63	0.01	-2	≤ 23.89	-	0.08
LP916-45	238.90352	-32.00020	M4	5000	-1	19.3	2-	92.92±13.88	66.49,119.35	0.28	-	≤ 10.25	-	0.25
LHS411	240.71045	+20.58700	M4	5000	-1	10.0	7-	7.30±0.90	3.43,18.14	0.27	-2	≤ 10.25	-	0.25
GJ3942	242.26375	+52.94399	M0	5000	-1	19.9	4-	291.95±2.31	267.38,328.17	0.04	5,3	30.24±0.77	14.53,22.78	0.17
G180-42	243.48382	+33.77325	M2.8	5000	-9	22.5	1-	90.40±9.77	81.91,94.36	0.02	1,3	51.07±3.75	36.75,38.17	0.14
G1625	246.35404	+54.30377	M2.1	5000	-1	17.1	3-	14.98±1.15	13.79,16.68	0.05	-2	≤ 2.69	-	0.23
LP386-49	246.38438	+26.02716	M3	5000	-1	17.1	2-	55.65±8.19	38.04,73.25	0.32	-2	≤ 25.09	-	0.16
G225-64	247.76367	+64.68455	M1	5000	-1	18.3	2-	52.35±9.28	45.38,59.31	0.13	-2	≤ 28.05	-	0.03
GJ3959	247.82792	+40.86492	M5	5000	-2	6.4	3,1-	10.73±0.16	5.53,49.80	0.14	15,1	4.03±0.17	2.16,16.72	0.17
GJ3966	248.86455	+35.01575	M2	5000	-1	11.6	3-	101.21±3.83	80.78,119.65	0.16	2-	22.43±3.12	21.99,22.86	0.02
LTT14949	250.20340	+36.31705	M4	5000	-1	19.2	2-	77.81±8.67	64.66,90.98	0.17	-	≤ 34.43	-	0.29
LHS3240	251.55658	+16.47710	M2.5	5000	-1	16.6	-	1.41±0.36	1.34,1.48	-	-	-	-	-
LHS3241	251.63054	+34.58133	M6.5	5000	-1	10.6	2-	805.54±21.48	706.99,852.56	0.05	-	39.96±4.78	24.11,46.17	0.07
G181-10	252.35314	+39.27570	M0	5000	-1	22.6	5-	13.15±1.50	4.48,23.07	0.25	-2	≤ 7.59	-	0.13
GJ3976	252.74154	-22.45238	M4.9	5000	-9	8.7	20,-	69.76±0.46	44.04,164.09	0.13	4-	16.38±1.53	9.55,25.64	0.19
GJ1207	254.27479	-4.34962	M4.1	5000	-9	13.1	4-	26.65±3.19	19.31,38.06	0.12	1,2	23.63±2.79	0.00,0.00	0.09
GJ3981	254.60467	+13.96969	M4	5000	-1	13.1	4-	-	19.31,38.06	-	-2	≤ 4.33	-	0.04
LTT15087	257.38233	+43.68079	M3.9	5000	-9	7.5	-	16.57±3.70	15.55,17.57	0.06	1,1	15.35±3.50	15.19,15.51	0.01
GJ3997	258.95853	+19.00004	M0.5	5000	-1	12.0	2-	90.76±7.58	66.86,114.67	0.26	-	≤ 28.83	-	0.05
LP447-38	259.59348	+18.14858	M3	5000	-1	20.0	3-	46.21±7.82	42.44,48.96	0.04	-2	-	-	-
LHS3281	259.97038	+41.71221	M2.7	5000	-1	12.4	6-	15.94±1.52	11.59,20.91	0.13	-3	≤ 17.80	-	0.11
GJ669A	259.97537	+26.50155	M3.4	5000	-13	5.0	9-	30.17±0.50	22.60,60.62	0.07	7-	9.53±0.54	5.96,17.42	0.24
G1678-1A	262.59475	+5.54805	M0.5	5000	-9	10.0	5-	135.73±4.51	129.84,148.57	0.02	-	-	-	-
G1686	264.47418	+18.59363	M1.2	5000	-9	8.1	3-	47.19±2.30	29.05,60.05	0.14	-2	≤ 9.47	-	0.46
LHS3321	265.98320	+43.37744	M2.6	5000	-1	19.4	4-	31.34±2.39	21.95,38.37	0.12	-4	≤ 9.44	-	0.15
GJ693	266.63859	-57.32167	M2	5000	-1	19.4	2-	26.71±7.38	23.37,30.03	0.12	-2	≤ 25.82	-	0.10
NTT45468	267.89759	+37.82702	M5.5	5000	-1	17.6	1,1	50.46±7.84	47.08,53.81	0.03	-2	≤ 3.34	-	0.11
G227-22	270.57009	+64.26163	M6.1	300	13,13	7.1	2-	24.68±2.07	18.98,30.38	0.23	2-	10.23±1.91	0.00,0.00	0.56
G182-37	271.07349	+35.95665	M0.5	5000	-1	21.4	2-	240.13±19.56	239.33,240.89	0.00	1,1	38.70±8.83	35.72,41.67	0.08
G1701	271.28269	-3.03197	M1	5000	-2	7.8	2-	54.74±4.18	52.88,56.61	0.03	-	-	-	-
LP449-10	271.70238	+17.34677	M4	5000	-1	17.7	2-	5.64±1.34	5.16,6.14	0.09	-	-	-	-
G204+55	274.12949	+45.55851	M0.6	5000	-9	17.1	3-	192.28±11.12	184.22,208.14	0.00	1,2	24.64±2.75	0.00,0.00	0.19
GJ4053	274.74070	+66.19169	M4.5	5000	-1	7.3	4-	9.32±1.11	7.14,11.59	0.21	1,3	7.00±0.63	0.00,0.00	0.17
NTT46734	277.98401	+77.51048	M4.5	5000	-1	23.2	3-	127.07±6.18	58.38,195.66	0.54	1,1	87.60±13.78	0.00,0.00	0.05
G205-28	277.99309	+40.68702	M3.5	5000	-1	13.2	4-	25.94±2.88	16.06,30.93	0.25	-	-	-	-
G141-21	279.08050	+33.61678	M4.1	5000	-9	10.2	2-	44.06±4.41	34.86,53.26	0.21	-2	≤ 11.10	-	0.28
G206-37	279.99972	+33.41553	M3.5	5000	-1	21.8	2-	131.44±15.40	41.06,221.84	0.69	-	-	-	-
GJ725A	280.68937	+59.63392	M3	5000	-1	3.6	2-	14.52±0.78	11.73,17.31	0.19	2-	1.91±0.43	1.39,2.44	0.27
G1725B	280.69055	+59.63028	M3.5	5000	-1	3.5	2-	4.62±0.48	4.50,4.75	0.03	-2	≤ 1.15	-	0.08

TABLE 1—Continued

Name ^a	RA J2007 (deg)	DEC J2007 (deg)	SpT	Age ^b (Myr)	Ref	Dist. (pc)	NUV det ^c , u.l.d	NUV μ^e (μ Jy)	NUV Min,Max ^g (μ Jy), (μ Jy)	NUV MAD rel ^f	FUV det ^c , u.l.d	FUV μ^e (μ Jy)	FUV Min,Max ^g (μ Jy), (μ Jy)	FUV MAD rel ^f
LHS3412	282.21530	+17.43813	K7	5000	-1	17.1	7-	576.00±13.58	510.08,649.03	0.06	1.3	36.41±3.43	22.28,32.05	0.16
G1729	282.45703	-23.83660	M4.1	5000	-9	3.0	2-	22.98±0.68	20.91,25.05	0.09	2-	6.18±0.71	5.54,6.83	0.10
G205-38	282.68910	+47.97186	M3.5	5000	-10	18.9	9-	11.70±1.39	6.43,18.68	0.18	-8	≤ 23.52	-	0.30
LHS3420	283.14111	+45.64304	M5	5000	-10	21.5	3-	48.53±6.31	21.68,67.07	0.18	-8	-	-	-
G1745A	286.77218	+20.87737	M2.1	5000	-9	8.5	2-	9.80±1.99	8.73,10.87	0.11	-2	≤ 7.82	-	0.25
G1745B	286.80401	+20.87636	M2.1	5000	-1	8.8	2-	11.02±1.13	8.83,13.22	0.06	1.1	9.71±1.83	9.16,10.25	0.06
LHS3472	293.73000	+53.25729	M2.5	5000	-1	13.9	2-	11.89±3.69	8.83,13.22	0.05	-2	≤ 19.85	-	0.39
LP869-42	294.90152	-26.75247	M1	5000	-1	22.3	2-	250.60±23.79	249.49,251.73	0.00	-2	≤ 83.31	-	0.49
NTT48178	296.22470	-23.63340	M5	5000	-1	9.2	4-	21.81±2.27	16.96,27.01	0.14	2.2	9.48±2.20	5.08,15.00	0.33
NTT48492	299.46590	-10.88529	M4.5	5000	-3	15.3	7-	55.28±4.41	41.36,74.28	0.22	-4	≤ 22.88	-	0.20
NTT48651	301.12851	-23.70119	M4.5	5000	-1	12.8	9-	117.85±3.71	68.71,221.13	0.20	3-	29.64±3.65	15.27,54.69	0.18
NSV13092	306.92316	-27.74940	M3	5000	-1	10.1	9-	28.62±1.12	21.18,38.27	0.03	-2	≤ 12.78	-	0.15
GJ791.2	307.45275	+9.68921	M	5000	-1	8.8	2-	37.04±3.09	34.14,39.94	0.08	2-	≤ 22.88	-	0.21
NTT49465	307.63559	+65.45011	M3	5000	-6	8.0	2-	44.84±3.39	44.30,45.38	0.01	-2	≤ 5.94	-	0.40
LHS3474	308.62984	-32.51693	M3	5000	-1	17.3	6-	28.43±3.38	20.83,35.08	0.17	-3	≤ 15.06	-	0.05
NTT50171	311.09141	+19.74852	M3	5000	-1	20.0	6-	498.95±25.55	432.24,565.64	0.13	-2	388.78±15.26	309.92,448.07	0.10
AU Mic	311.29035	-31.34160	M1	5000	-1	10.0	4-	2037.27±19.21	1677.87,2422.63	0.11	3-	31.84±5.76	26.39,37.28	0.17
LHS3576	311.68239	-11.80380	M4.5	40	7,13	14.6	2-	87.94±6.48	85.22,90.66	0.03	2-	-	-	-
LHS3666	312.41523	-0.35127	M3.5	5000	-1	21.2	2-	36.60±8.02	34.52,38.70	0.06	-	-	-	-
LP636-16	313.13108	-1.78594	M	5000	-1	24.5	2-	19.06±4.29	18.07,20.05	0.05	-	-	-	-
NTT50171	314.11371	-24.00366	M	5000	-1	16.1	7-	21.88±3.26	11.72,26.62	0.07	-4	≤ 65.67	-	0.23
NSV13417	314.19410	-10.45070	M2.8	5000	-9	15.2	3-	37.32±4.90	30.10,41.10	0.01	1.2	16.51±2.38	12.52,18.97	0.05
LHS3612	315.49390	-6.31961	M3	5000	-1	13.8	5-	43.32±2.72	38.89,48.07	0.07	-2	≤ 20.36	-	0.11
NTT50710	317.80684	-22.80548	M	5000	-1	15.7	3-	39.33±4.88	21.94,49.45	0.06	-2	≤ 16.13±5.19	14.25,18.02	0.12
HD 201919	318.27212	-17.48711	K5	100	15,13	22.6	2-	1050.34±33.72	1022.54,1078.16	0.03	2-	148.21±23.19	144.29,152.16	0.03
21763528-6005124	319.14700	-60.08678	M3.9	40	7,7	27.0	5-	248.04±16.29	140.48,504.69	0.26	2.2	99.16±10.35	50.08,230.22	0.11
LTT8526	321.96074	-68.68442	M4.1	40	7,7	28.1	4-	107.56±9.55	74.54,153.89	0.14	-	≤ 25.87	-	-
G1829	322.39143	+17.64403	M2.5	5000	-6	6.7	3-	16.39±1.69	13.99,19.94	0.08	-2	≤ 7.03	-	0.14
G1832	322.40544	+17.64403	M4	5000	-1	5.0	2-	39.65±1.37	38.83,40.48	0.02	-2	4.26±0.80	4.13,4.39	0.03
21370885-6036054	324.28704	-60.60170	M3.6	40	7,7	23.4	5-	299.98±13.34	216.51,385.54	0.20	2-	65.14±13.79	57.17,73.10	0.12
LHS513	324.75554	-24.15918	M4	5000	-1	15.1	7-	7.09±0.59	3.01,21.55	0.18	1.7	4.18±0.20	2.26,7.96	0.31
21504048-5113380	327.66867	-51.22722	M4.2	40	7,7	25.9	3-	82.41±12.50	75.67,88.48	0.06	-3	≤ 91.76	-	0.04
LP518-58	330.30552	+13.60406	M4.5	5000	-1	13.5	7.2	6.16±0.45	3.95,9.31	0.22	3.8	3.55±0.16	2.75,3.08	0.12
GJ4247	330.30552	+13.60406	M4	5000	-1	8.9	2-	294.09±8.09	192.84,395.23	0.34	2-	110.17±7.82	81.88,138.46	0.26
LHS3744	330.45515	+16.46776	M2	5000	-1	16.4	2-	131.17±11.16	127.89,134.45	0.03	2-	49.44±11.55	36.90,61.97	0.25
LHS3744	330.50483	-19.48299	M3.5	5000	-1	12.8	2-	9.29±2.75	8.40,10.17	0.09	-3	≤ 9.38	-	0.06
22025453-6440441	330.72744	-64.67910	M2.1	40	7,7	28.3	2-	608.38±34.68	601.07,615.64	0.01	-3	128.37±23.85	123.90,132.79	0.03
LTT8848	331.46322	-11.91451	M0	5000	-1	20.0	4-	351.35±11.92	331.16,360.72	0.01	1.2	29.66±5.41	26.88,35.16	0.00
G214-14	332.82010	+41.01569	M2	5000	-1	22.3	4-	118.97±15.45	79.52,158.59	0.18	-4	≤ 72.49	-	0.24
LHS3776	333.42998	-17.68620	M4.5	5000	-1	10.4	81.1	2.36±0.08	0.95,28.49	0.25	4.79	2.33±0.03	0.55,13.68	0.32
GJ4274	335.77955	-17.60868	M4	5000	-1	7.4	4-	36.48±1.97	27.17,45.12	0.17	-	≤ 9.16	-	0.15
LHS3804	336.27221	-47.88070	M3.5	5000	-1	11.9	4-	11.78±1.96	9.19,14.74	0.14	-2	≤ 16.82	-	0.14
LP876-34	337.19175	+18.93145	M1	5000	-1	15.6	2-	219.36±18.61	210.99,227.70	0.04	-	≤ 16.82	-	0.14
G127-35	338.50173	-25.24301	M2	5000	-1	3.5	4-	5.92±0.33	4.50,8.21	0.12	-2	2.42±0.33	1.90,2.83	0.09
EZ Aqr	339.64520	-15.29480	M5.5	5000	-1	19.3	3-	52.51±5.34	14.86,123.89	0.21	4-	≤ 5.66	-	0.18
LP156-37	340.30825	-10.74647	M4.5	5000	-1	21.2	6-	76.04±6.71	45.93,91.91	0.06	-3	≤ 37.07	-	0.14
LHS528	340.66373	+17.67024	M2.5	5000	-1	16.4	6-	20.01±2.32	13.07,26.92	0.20	-4	≤ 15.48	-	0.31
GJ4292	340.84720	+22.13833	M4.5	5000	-1	23.7	-	-	13.07,26.92	0.20	-2-	159.62±20.85	149.30,169.97	0.06
VW P8A	341.24196	-33.25071	M4	12	14,16	23.7	-	-	13.07,26.92	0.20	2-	13.38±2.25	12.60,14.16	0.06
LTT54721	341.25063	-33.25740	M5	5000	-1	8.3	-	-	13.07,26.92	0.20	2-	93.37±12.01	59.90,106.18	0.23
22463471-7353504	341.64504	-73.89747	M3.2	40	7,7	27.5	-	-	228.46,426.83	0.10	4.1	≤ 39.78	3.94,10.96	0.16
LHS3854	341.64504	-73.89747	M3	5000	-1	23.1	5-	21.42±3.85	9.50,29.72	0.23	-3	7.86±1.41	0.24	0.24
NTT54872	342.01934	-24.36910	M4	5000	-1	7.2	5-	39.60±1.70	31.04,55.67	0.14	3-	≤ 50.73	-	0.05
LHS3856	342.09469	+12.53621	M	5000	-1	20.1	3-	39.70±6.75	16.24,70.58	0.50	-3	14.10±2.16	13.70,14.74	0.01
HD 216133	342.58073	-7.08990	M0.2	5000	-9	14.0	7-	197.67±2.64	36.24,41.26	0.06	-2	≤ 32.74	-	0.14
LHS3859	342.65909	+34.85668	M1.5	5000	-1	19.0	2-	38.74±8.64	16.16,49.80	0.40	-4	≤ 28.62	-	0.07
LP344-47	342.68995	+28.60228	M3	5000	-1	20.9	3-	33.84±6.93	30.28,45.50	0.20	2-	93.73±11.80	78.44,109.01	0.16
CT Peg	342.97426	-31.75411	M2.7	300	13,13	14.3	3-	394.42±11.01	302.85,503.70	0.30	-2	≤ 37.93	-	0.02
LP401-10	343.54708	+25.46590	M5.5	5000	-1	23.2	2-	67.56±15.09	41.28,93.82	0.29	-2	5.67±1.12	5.51,5.83	0.03
G1877	343.93166	-75.46073	M3	5000	-5	8.6	2-	28.08±2.29	27.21,28.95	0.03	1.1	-	-	-

NOTE.—In the reference column, the first number is the spectral type reference and the second is the age reference. Reference numbers: 1. Reid et al. (2007) 2. Reid et al. (1995), Hawley et al. (1996), 3. Alonso-Floriano et al. (2015) 4. Gray et al. (2003), 5. Gray et al. (2006), 6. Jenkins et al. (2009), 7. Kraus et al. (2014), 8. Lépine et al. (2014), 9. Mann et al. (2015), 10. Newton et al. (2014), 11. Rajpurohit et al. (2013), 12. Scholz et al. (2005), 13. Shkolnik et al. (2009), 14. Shkolnik et al. (2012), 15. Shkolnik et al. (2014), 16. Torres et al. (2006) 17. Schlieder et al. (2012). The star GJ447 has several literature estimates for its age. Montes et al. (2001) determined that it is a member of the Ursa Major moving group (300 Myr) with a radial velocity (RV) of -13.0 ± 5.0 km/s. However, King et al. (2003) does not confirm the membership with a RV measurement of -29.0 ± 1.2 km/s, which is consistent with the RV standard list of Nidever et al. (2002) (-31 ± 0.1 km/s).

^a2MASS designation

^bIf no age is provided by the literature, the star is assumed to be 5 Gyr old.

^cdet - detections

^du.l. - upper limits

^e μ = Mean flux density values are scaled to 10 parsecs.

^fMAD rel- median absolute deviation (MAD) divided by the median indicated by MAD_{rel} in our plots

^gMinimum and maximum flux density scaled to 10 parsecs

^hIRXS source, there is only one

2.1. GALEX Photometry

The *GALEX* pipeline performs photometry on all recognized sources within the field of view for every exposure (Morrissey et al. 2007). We queried the archive¹ for all observations within a 5'' radius centered around a target's proper motion corrected coordinates. If the cone search yielded multiple observations for a target at the same point in time, the observation closest to the coordinates were taken. Detections with a signal-to-noise of less than two were removed. *GALEX* observed 55% of the stars in our target list. In the NUV band, 36% of the targets had at least two observations. In the FUV, 30% were observed two or more times. Known spectroscopic binaries, visual binaries and background galaxies within the 5'' *GALEX* NUV point spread function were removed from our analysis.

A non-linear response is recorded on the *GALEX* detector when a count rate over 108 counts/s in the NUV or 34 counts/s in the FUV was reached (Morrissey et al. 2007). 2034 observations were taken in the NUV band. One NUV data point was removed for non-linearity and 54 were removed due to either reflections or ghosting on the NUV detector.² There were 1403 FUV observations and only one point was removed for non-linearity. After these cuts, we were left with 357 and 303 stars with at least two reliable observations in the NUV and FUV band, respectively. At total of 1497 NUV and 1035 FUV observations were used in this analysis. Stars that are M5 and earlier represent 96% of the stars with multiple detections in both photometric bands. None of the eight M8 or later stars from the original list have multiple *GALEX* detections (Figure 1). Two examples of NUV and FUV light curves are shown in Figure 2.

The reported quantities from the *GALEX* pipeline were used to estimate the upper limits, ensuring that all flux limits were extracted and calibrated in the same fashion. The 2σ errors from nearby detections within 10' and no *GALEX* artifact flags can be used to estimate the upper limit of a non-detection. Upper limits were calculated

for 0.9% of the NUV and 59% of the FUV observations for stars in our sample with multiple detections. The non-detection rate is 1% higher in both bands when considering stars with at least one detection. With these detection rates, we achieved a volume limited sample in the NUV. The sample in the FUV is magnitude limited and we discuss the effect of this in Section 3.2.

3. Variability Analysis

The median number of detections for the NUV and FUV band is 3 and 1 respectively (Figure 3). This makes it difficult to characterize specific sources of a star's variability for each target such as rotation, flaring or changes in its activity cycle. For those with at least two observations, the time span between observations ranges from two minutes to the full eight year mission. In order to systematically study the variability of the sample we computed the median absolute deviation divided by the median (MAD_{rel}) for the NUV and FUV flux densities for each target. We also report the maximum and minimum flux densities for each star in Table 1. Note that the minimum flux density may be from a detection or an upper limit.

The *GALEX* pipeline calibrates flux densities and magnitudes to 18 white dwarf standards (Morrissey et al. 2007), which are assumed to be invariant and ideal UV flux calibrators (Harris et al. 1988). However, we still measure variability in the light curves of the 18 *GALEX* standard white dwarfs and the white dwarfs from the Villanova Catalog of Spectroscopically Identified White Dwarfs (McCook & Sion 1999). We calculated the MAD_{rel} of 1225 white dwarfs in the NUV and 952 white dwarfs in the FUV to cover a wide range of *GALEX* magnitudes.³ We measured MAD_{rel} to be 2.1% and 3.5% for the NUV and FUV band, respectively. These photometric errors were added to the MAD_{rel} uncertainties for all target stars in our analysis.

A summary of the variability results for individual targets with multiple detections are listed in Table 1. The results binned by spectral type are listed in Table 2

¹<http://galex.stsci.edu/casjobs/>

²<http://galex.stsci.edu/gr6/?page=ddfaq>

<http://www.galex.caltech.edu/wiki/>

Public:Documentation/Chapter.8#Setting_the_Ghost_Flag

³Pulsating white dwarfs, binary systems, and suspected planetary nebula were removed from the sample.

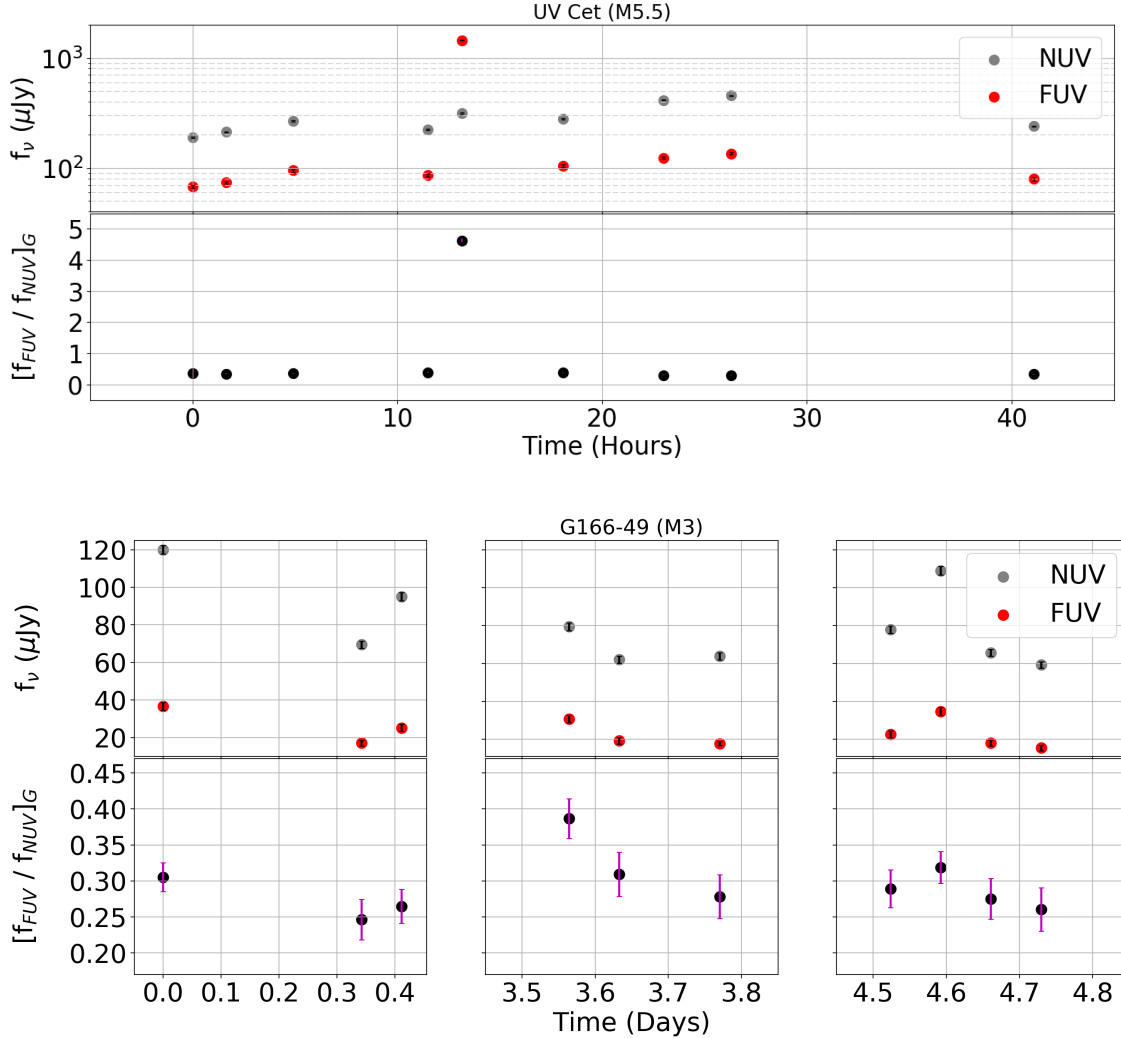


Fig. 2.— NUV (grey) and FUV (red) observed flux density light curves for UV Cet (top) and G166-49 (bottom). The ratio of FUV to NUV flux density ($[f_{FUV} / f_{NUV}]_G$) is plotted with black dots below the light curves. The error bars are shown on the data points in black and magenta, for the flux densities and flux density ratios respectively. The units of time are different between both light curves. The NUV and FUV flux densities are typically correlated, but there is a strong flare on UV Cet where the FUV emission spikes compared to the NUV emission.

3.1. NUV Variability

For stars with multiple observations, the median MAD_{rel} in the NUV band is 11%, with the largest observed change at 76%. Within each spectral type bin, there is a wide range of variability, with the span increasing with later spectral type (Figure 4). M0s have a median variation of 4% and M4s have a median variation of 16%. The

K7, M6, and M7 bins are each represented by less than a dozen stars. The remaining bins each have between 20 and 85 stars (Figure 1).

Fifteen percent of the stars with multiple NUV detections are young (≤ 300 Myr). Young stars are known to have higher levels of UV emission in the *GALEX* bandpasses relative to older stars (Shkolnik et al. 2011; Stelzer et al. 2013; Shkol-

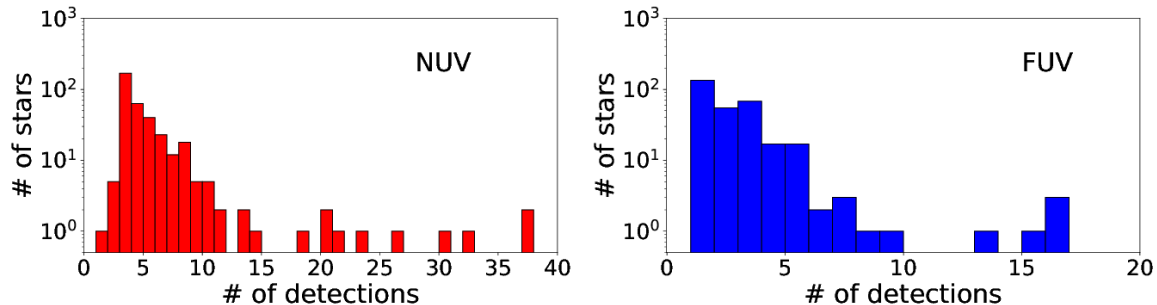


Fig. 3.— Histogram of the number of detections for each *GALEX* band. LHS 3776, which has 81 detections in the NUV was left off of the histogram.

nik & Barman 2014). We observe no significant difference between the median variability for each spectral type between the old and young populations.

The ratio of maximum flux density to minimum flux density (MAX/MIN) has a larger spread and amplitude at later spectral types in the NUV band (Figure 5). The four stars with a MAX/MIN ratio >10 are GJ1167A, GJ3856, LHS3776, and LHS5226. The largest MAX/MIN value was 76.3, produced by GJ1167A. In the case of these stars, there are distinct flares in the light curves. This is indicated by sharp changes over the course of hours or large deviations from the apparent baseline of each star.

3.2. FUV Variability

We performed the same variability analysis for the FUV observations as we did for the NUV twice, with and without upper limits because 59% of the observations were non-detections. The FUV variability spans from 0.1% to 88% when the upper limits are included. The median activity in the FUV bandpass is 16%, which is slightly higher than the NUV value. The distribution of FUV variability without upper limits falls completely within the NUV distribution, although the median activity is higher (Figure 6). The maximum range of MAD_{rel} goes down to 57% when the upper limits are removed. In the latter case, the data may be biased to only the brightest and perhaps most active FUV emitters. There remains no significant difference between old and young stars for the overall median levels of variability across spectral types. There is a slight trend between

increased variability and later spectral type when upper limits are included, but no clear trend between variability and spectral type when the upper limits are excluded (Figure 4). The spread in variability between the NUV band and FUV band (with and without upper limits) for each spectral is not significantly different (Figure 7).

The ratio of maximum flux density to minimum flux density (MAX/MIN) has a larger spread and amplitude at later spectral types in the FUV band (Figure 5). The four stars that have a MAX/MIN ratio >10 are GJ1167A, LHS3776, LHS5094, and UV Cet. The FUV light curves of these stars also show evidence of flaring based on sharp hourly changes and/or large deviations from an apparent baseline. LHS5226 and GJ3856 do not have detections or upper limits in the FUV despite having relatively high NUV MAX/MIN values. LHS3776 has the largest MAX/MIN in the FUV with a value of 30.0, which is higher than its NUV MAX/MIN value of 24.7. Both LHS5094 and UV Cet have MAX/MIN values in the NUV but they have smaller values, 7.3 and 1.2 respectively.

4. *GALEX* FUV and NUV Correlations and Ratios

Correlations between activity indicators are useful in understanding the physics of stellar atmospheres, as well as providing tools with which to predict one activity diagnostic with the other when it is not observable or detectable. *GALEX* recorded 393 simultaneous NUV and FUV observations for 145 stars, providing a unique data set with which to search for correlations between the two activity indicators. Detections are consid-

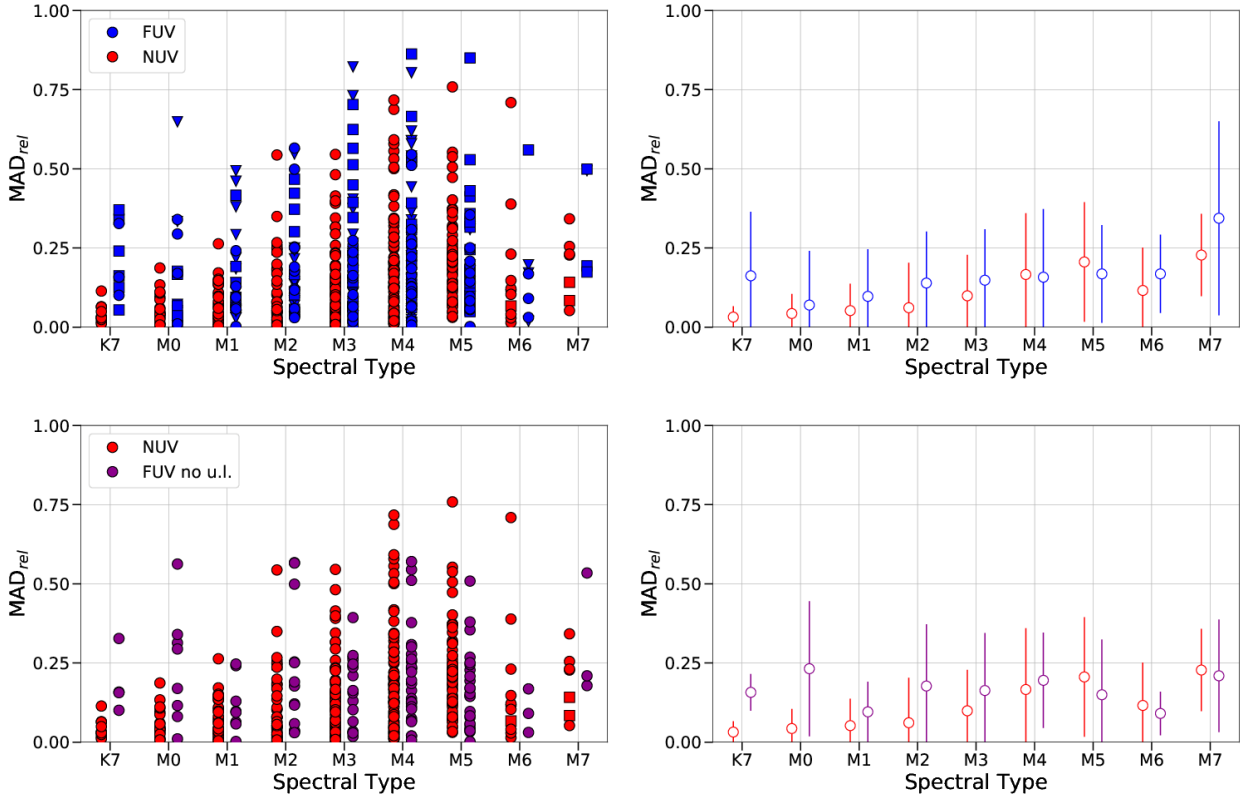


Fig. 4.— The relative median absolute deviation (MAD_{rel}) plotted against spectral type - *Top*: NUV band (red) and FUV band with upper limits (blue). *Bottom*: NUV band (red) and FUV band without upper limits (purple). *Left*: Triangles are used to indicate stars that have only upper limits. Squares are used for stars that have at least one upper limit. Dots represent stars with only detections. *Right*: The open circles are the median spectral type values for each band with the interquartile range plotted.

ered simultaneous by having the same *GALEX* reported time, which is precise down to the second. There are significantly fewer FUV detections than NUV detections because: (1) M dwarfs are typically less luminous in the FUV and (2) the *GALEX* FUV detector failed six years into the mission, while the NUV band continued operating for another four years.

We scaled the NUV and FUV detections to 10 pc and subtracted each observation by the photospheric contribution as done by Shkolnik & Barman (2014) to determine the “excess” emission from the stellar upper atmosphere (i.e., the chromosphere, transition region and corona). This is achieved by using the PHOENIX photospheric models (Hauschildt et al. 1997; Short & Hauschildt

2005) for a given stellar effective temperature and age.

We converted the published spectral type to effective temperature by interpolating the relationships measured by Luhman (1999) and Schmidt-Kaler (1982) and compiled by Kraus & Hillenbrand (2007). Ages were adopted from the literature with the references listed in Table 1. If there is no reported age for a star, we assume it to be the average age of the field, 5 Gyr. The differences are usually negligible between the observed and excess flux densities as shown in Figure 8. On average, the fraction of the model photospheric emission of the observed emission is 4% and $7 \times 10^{-4}\%$ in the NUV and FUV bands, respectively. As discussed earlier, previously published correlations rely on

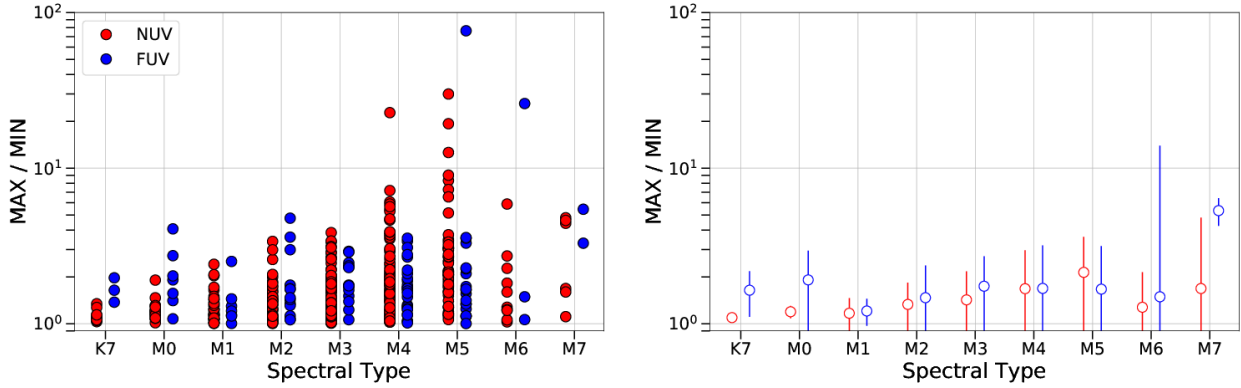


Fig. 5.— The ratio of the maximum flux density to the minimum flux density (MAX/MIN) plotted against spectral type for the NUV (red) band and FUV (blue) band with upper limits. *Left*: Dots represent individual stars with MAX/MIN measurements derived from detections. Triangles represent stars where the minimum flux density is estimated with an upper limit. *Right*: Median MAX/MIN value for each spectral type plotted with the interquartile range. The ratio for each star is reported in Table 1.

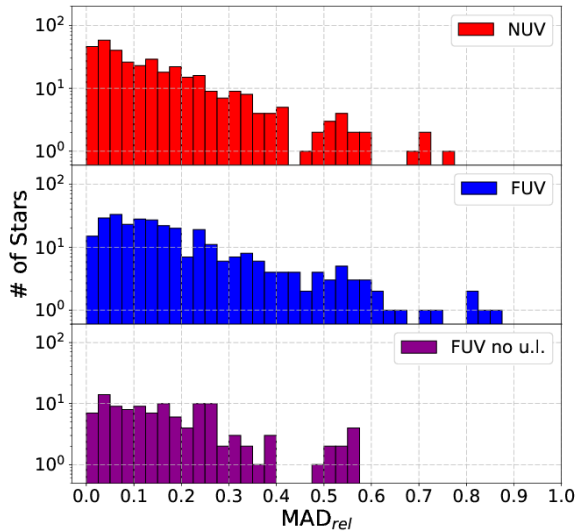


Fig. 6.— Histogram of the relative median absolute deviation (MAD_{rel}) for the NUV and FUV bands. FUV is shown with and without upper limits

data sets taken at different times, which introduces excess scatter due to varying activity levels between observations. In Figure 9, we plot all the NUV excess flux densities with simultaneous FUV detections scaled to 10 pc (f_{FUV} , f_{NUV}). A least

squares fit to the excess flux densities produces the following correlation:

$$\log(f_{FUV}) = A \log(f_{NUV}) + B \quad (1)$$

where constants A and B are 0.75 ± 0.04 and -0.14 ± 0.07 , respectively.

The range of excess flux density covers three orders of magnitude (Table 3, Figure 9) with the M3 – M5 population spanning the entire range of UV emission. K7 – M1 stars have the highest levels of NUV and FUV excess flux densities, and deviate the most from the collection of stars. Figure 10 (top) shows the scaled NUV and FUV observed flux densities plotted against effective temperature. There is an increase of flux density with effective temperature in both *GALEX* bands with young (≤ 300 Myr) stars emitting more emission than older stars. These trends are consistent with the work of Shkolnik & Barman (2014) and Ansdell et al. (2015), who used averaged *GALEX* flux densities. Despite later M stars showing more variability (in the NUV), they emit less excess UV emission in both *GALEX* bands.

Figure 10 (bottom) shows the ratio of the observed FUV to NUV fluxes as a function of effective temperature. The ratio of the integrated fluxes for the *GALEX* FUV and NUV bands are denoted by $[F_{FUV}/F_{NUV}]_G$ and the ratio of the flux densities are denoted by $[f_{FUV}/f_{NUV}]_G$. Note

TABLE 2
 MEDIAN MAD_{rel} FOR EACH SPECTRAL SUBCLASS.

SpT	NUV w/ u.l. ^a # stars	NUV w/ u.l. MAD_{rel}	FUV w/ u.l. # stars	FUV w/ u.l. MAD_{rel}	FUV w/o u.l. ^b # stars	FUV w/o u.l. MAD_{rel}
K7	10	0.03 ± 0.03	9	0.16 ± 0.20	4	0.16 ± 0.06
M0	20	0.04 ± 0.06	16	0.07 ± 0.17	8	0.23 ± 0.21
M1	36	0.05 ± 0.08	27	0.10 ± 0.15	8	0.10 ± 0.10
M2	45	0.06 ± 0.14	38	0.14 ± 0.16	13	0.18 ± 0.19
M3	75	0.10 ± 0.13	68	0.15 ± 0.16	17	0.16 ± 0.18
M4	82	0.17 ± 0.20	75	0.16 ± 0.22	29	0.20 ± 0.15
M5	52	0.21 ± 0.19	49	0.17 ± 0.15	24	0.15 ± 0.17
M6	11	0.12 ± 0.14	7	0.17 ± 0.12	3	0.09 ± 0.07
M7	7	0.23 ± 0.13	4	0.34 ± 0.31	3	0.21 ± 0.18
Overall	357	0.11	303	0.15	114	0.16

^aw/ u.l. - with upper limits

^bw/o u.l. - without upper limits

NOTE.—The errors on the MAD_{rel} quantity are the interquartile range. For each bandpass, the overall number of stars does not add up to sum of the stars in each spectral type column because 18 of the stars are identified as M dwarfs, but do not have a published subclass.

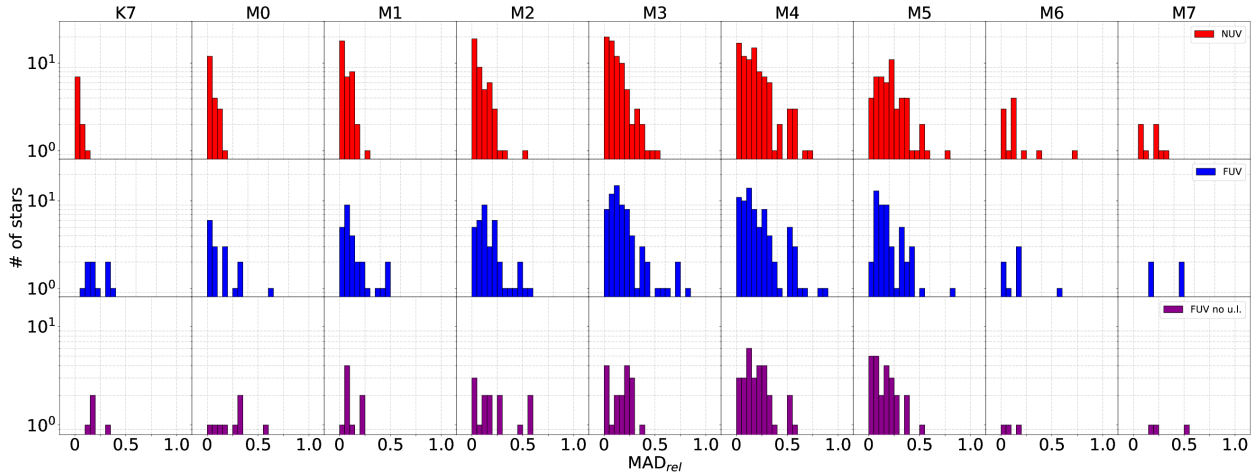


Fig. 7.— Histogram of the relative median absolute deviation (MAD_{rel}) for each spectral type. *Top*: NUV band. *Middle*: FUV band with upper limits. *Bottom*: FUV band without upper limits.

that the FUV band does not include the Lyman- α line where M dwarfs emit a significant portion of energy (Linsky et al. 2013). Although cooler stars produce less UV emission overall, both integrated and flux density ratios decrease at higher effective

temperatures (Figure 10; bottom). This trend has also been seen in work by France et al. (2016). The average *GALEX* flux density ratios for G types stars is 0.01 (Shkolnik 2013), whereas the average flux density ratio for our sample is 31 times higher

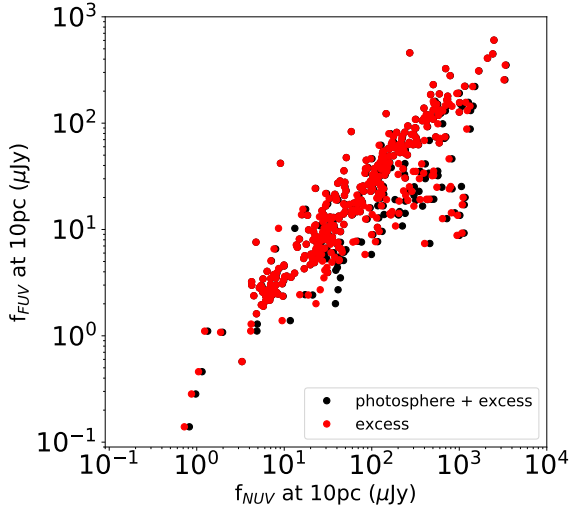


Fig. 8.— FUV flux density (f_{FUV}) at 10 pc vs. NUV flux density at 10 pc (f_{NUV}). The black dots are the original data and the red dots are the excess flux density.

with a ratio of 0.31.

Welsh et al. (2006) analyzed time-tagged GALEX data for four M dwarfs from a guest investigator program that monitored each star for 20 to 30 minutes. Their data shows distinct flares in the NUV and FUV. During these flares, the $[f_{FUV}/f_{NUV}]_G$ ratio increases from 0.5 to 13 on the timescale of minutes with clear flare onset occurring at about $[f_{FUV}/f_{NUV}]_G=1$. In our data set, $[f_{FUV}/f_{NUV}]_G$ spans from 0.008 to 4.6 and the 5 $[f_{FUV}/f_{NUV}]_G$ ratios that are >1 are likely due to flaring.

Nine stars with at least five simultaneous NUV and FUV detections were investigated individually to see how well their observations match the best fit line found using all simultaneous data of the same spectral type. The FUV and NUV flux densities of these stars are plotted in Figure 11. Five of the stars show comparable correlations to their respective spectral type, but four have observations which appear as a scatter plot. For three of the nine stars, we observe an order of magnitude spread in emission in one or both of the GALEX bands. UV Cet (M5.5) and G166-49 (M3) have the highest signal to noise and time resolution of the nine targets (Figure 2). In Figure 11 (top),

all of UV Cet’s data points follow near the best fit line for M5s, except for one observation when only the FUV emission increases by an order of magnitude. This causes $[f_{FUV}/f_{NUV}]_G$ to jump from a baseline of ~ 0.5 to 4.6. Such a sharp increase in FUV activity over a few hours is most likely due to a flare.

5. Conclusions

We analyzed the 377 low-mass stars within 30 pc with multiple photometric observations in the GALEX archive to characterize the stellar variability with the NUV and FUV bandpasses. The timing between the observations for each target ranges from minutes to years with a median time between observations of about a year. There were simultaneous NUV and FUV observations for 145 of the stars, which we used to measure the correlation between NUV and FUV emission for each spectral type and the variations in the GALEX FUV to NUV ratio.

The summary of our findings includes:

UV Variability: The median variation as measured by the relative median absolute deviation (MAD_{rel}) in the NUV flux density is 11% for the entire sample, and 16% for the FUV flux density. The median level of stellar variability in the NUV bandpass increases with later spectral type, from 4% for M0s to 21% for M5s. When upper limits are included, there is a slight trend between increased variability and later spectral type for the FUV band. There is no clear trend with spectral type when upper limits are not used. The median variability is 16% for M0s and 15% for M5s. The variability in the NUV and FUV is not significantly different for the young stars (≤ 300 Myr) compared to the old stars in our sample. The ratio of maximum flux density to minimum flux density has a larger spread at later spectral types for both the NUV and FUV bands.

GALEX FUV and NUV Correlations: The excess FUV and NUV flux densities (i.e. with effective temperature dependent photospheric emission subtracted) are correlated for stars with spectral types between M1 and M6. In these cases, the NUV emission can act as a proxy for the FUV when there are no FUV observations or detections. K7, M0 and M7 stars show no clear correlation in our data set, possibly due to the low numbers

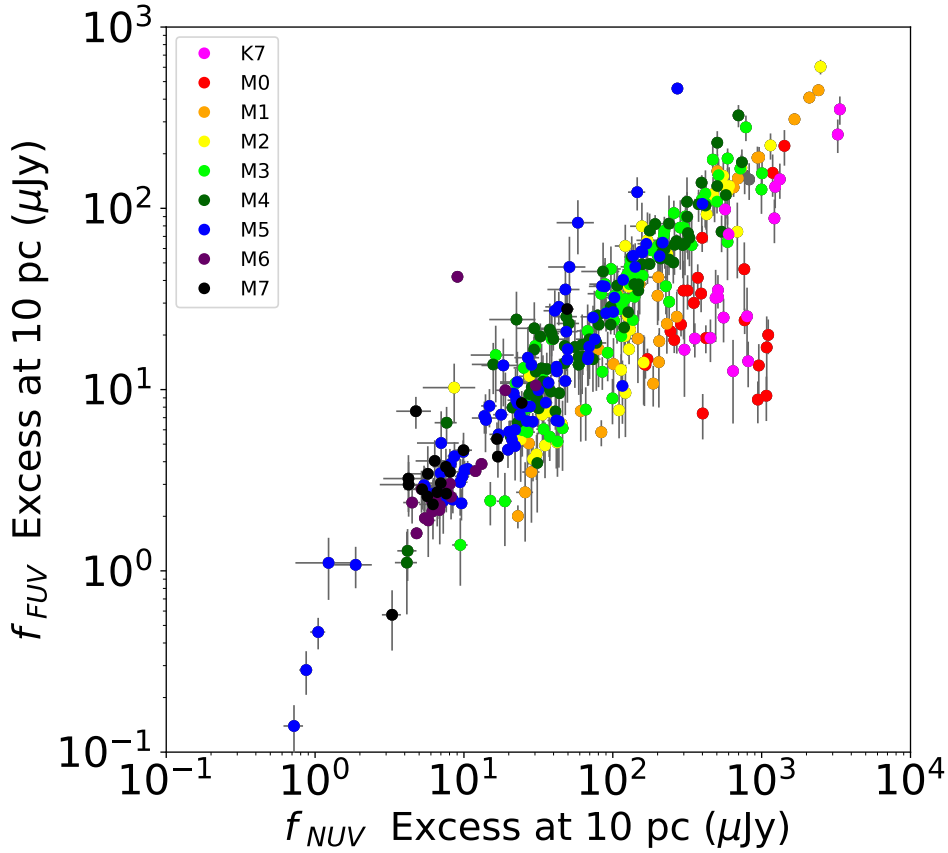


Fig. 9.— Simultaneously observed FUV excess flux density (f_{FUV}) vs. NUV excess flux density (f_{NUV}) with colors differentiating spectral types. Coefficients for the equations of the best fit line of each spectral type are listed in Table 3.

of stars in each bin and their narrower range in emission levels.

GALEX $[f_{FUV}/f_{NUV}]_G$ Ratio: The average of FUV to NUV flux density ratio of our low-mass stars are 31 times higher than the average for G-stars measured with *GALEX*, bolstering the need to measure such ratios for the low-mass stars that host HZ planets with atmospheres in which observers will seek oxygen. Tian et al. (2014) calculated that under these UV conditions, O_2 and O_3 could be 2-3 orders of magnitude greater than in the atmospheres of HZ planets around Sun-like stars producing a potential false-positive detection of a biosignature (Harman et al. 2015). In a few cases, likely during a flare, we see significant deviation of the *GALEX* $[f_{FUV}/f_{NUV}]_G$ ratio from the norm for a given star reaching levels >1 . We also observe that on average, *GALEX* $[f_{FUV}/f_{NUV}]_G$

and $[F_{FUV}/F_{NUV}]_G$ for each observation increases for later spectral types with. For M0s f_{FUV}/f_{NUV} has a median value of 0.08 and M4s has a median value of 0.28.

These results characterize the UV behavior for the largest set of low-mass stars to date. The statistical FUV and NUV variability levels, correlations and ratios will aid in our understanding of the high-energy radiation environment of exoplanets. Future studies with greater time resolution and temporal coverage should reliably distinguish between baseline emission and modulation due to rotation, flaring and stellar activity cycles, especially valuable for a particular exoplanetary system of interest. This will require building dedicated UV telescopes that can observe a sizable population of low-mass stars and monitor choice planet hosts for weeks at a time. Understanding

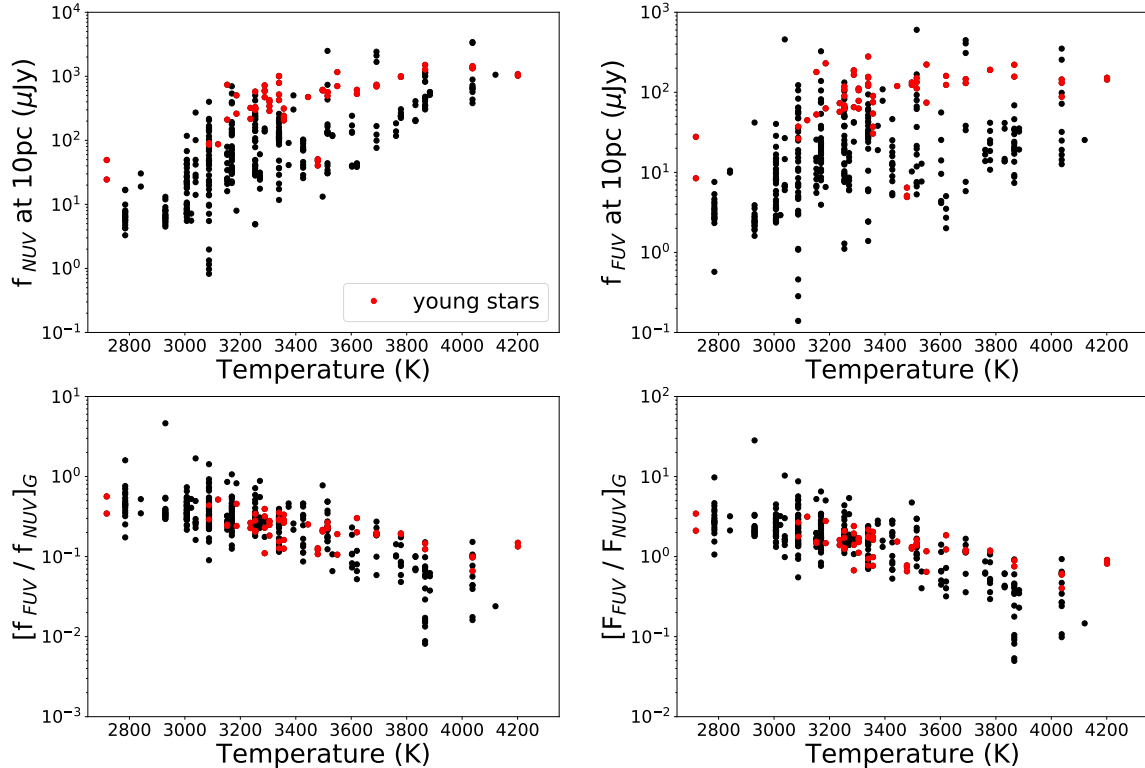


Fig. 10.— GALEX observed flux densities (f_ν) scaled to 10 pc for the NUV (top, left) and FUV (top, right) band plotted against effective temperature. The fraction of FUV to NUV observed flux density (bottom, left) and fraction of integrated band flux (F_ν) (bottom, right) plotted against effective temperature. Young stars are have ages less than 300 Myr old and labeled in red.

such stellar activity will become especially important when missions like the James Webb Space Telescope begin to search for biosignatures in the spectra of HZ planets around low-mass stars.

6. Acknowledgements

The authors would like to thank S. Flemming and T. S. Barman for useful discussion. B.E.M acknowledges the support of NSF grant AST-1461200 to Northern Arizona University and the National Institute of General Medical Sciences of the National Institutes of Health under award number R25GM055052 awarded to T. Hasson. The content is solely the responsibility of the authors and does not necessarily represent the official views of the National Institutes of Health. E.S. appreciates support from NASA/Habitable Worlds grant NNX16AB62G.

REFERENCES

- Alonso-Floriano, F. J., Morales, J. C., Caballero, J. A., et al. 2015, *A&A*, 577, A128
- Anglada-Escudé, G., Amado, P. J., Barnes, J., et al. 2016, *Nature*, 536, 437
- Ansdell, M., Gaidos, E., Mann, A. W., et al. 2015, *ApJ*, 798, 41
- Arney, G., Domagal-Goldman, S. D., Meadows, V. S., et al. 2016, *Astrobiology*, 16, 873
- Bochanski, J. J., Hawley, S. L., Covey, K. R., et al. 2010, *AJ*, 139, 2679
- Dressing, C. D., & Charbonneau, D. 2015, *ApJ*, 807, 45
- France, K., Froning, C. S., Linsky, J. L., et al. 2013, *ApJ*, 763, 149

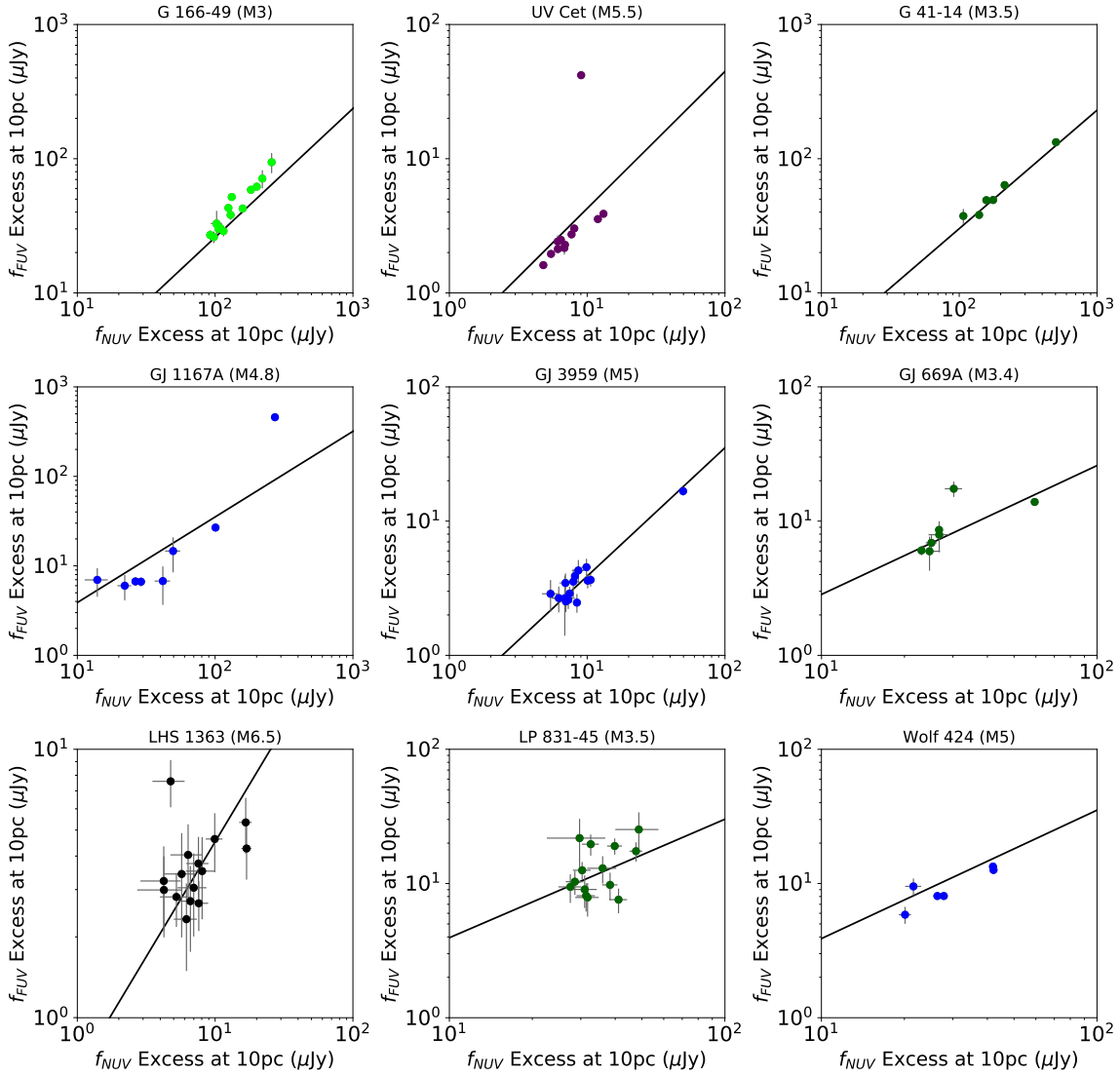


Fig. 11.— Plots of FUV flux density (f_{NUV}) vs NUV flux density (f_{FUV}) for individual stars. The black line in every figure is the best fit line of the fluxes for the corresponding spectral type using the coefficients in Table 3. Note: the x and y axis scales are different for most stars.

France, K., Parke Loyd, R. O., Youngblood, A., et al. 2016, ApJ, 820, 89

Gillon, M., Triaud, A. H. M. J., Demory, B.-O., et al. 2017, Nature, 542, 456

Gray, R. O., Corbally, C. J., Garrison, R. F., et al. 2006, AJ, 132, 161

Gray, R. O., Corbally, C. J., Garrison, R. F., McFadden, M. T., & Robinson, P. E. 2003, AJ, 126, 2048

Harman, C. E., Schwieterman, E. W., Schottekotte, J. C., & Kasting, J. F. 2015, ApJ, 812, 137

Harris, A. W., Gry, C., Bohlin, R. C., Blades, J. C., & Holm, A. V. 1988, in ESA Special Pub-

TABLE 3
 MEDIAN EXCESS FLUX DENSITY VALUES AT 10PC
 AND CORRELATIONS BY SPECTRAL TYPE

SpT	f_{NUVe}^a (μJy)	f_{FUVe} (μJy)	f_{FUVe}/f_{NUVe}	A ^b	B ^b
K7	600.4 \pm 890.3	32.3 \pm 92.2	0.06 \pm 0.04	1.24 \pm 1.54	-1.91 \pm 4.44
M0	398.6 \pm 383.1	20.9 \pm 49.3	0.08 \pm 0.05	0.34 \pm 1.12	0.50 \pm 3.00
M1	202.3 \pm 625.2	25.2 \pm 122.7	0.18 \pm 0.07	1.13 \pm 0.27	-1.14 \pm 0.63
M2	127.9 \pm 458.5	21.4 \pm 108.1	0.22 \pm 0.19	0.96 \pm 0.23	-0.59 \pm 0.49
M3	107.7 \pm 215.8	31.0 \pm 52.1	0.28 \pm 0.13	0.96 \pm 0.20	-0.51 \pm 0.41
M4	71.7 \pm 160.4	22.4 \pm 50.7	0.28 \pm 0.16	0.88 \pm 0.16	-0.29 \pm 0.31
M5	25.1 \pm 65.5	8.1 \pm 52.0	0.36 \pm 0.24	0.96 \pm 0.10	-0.37 \pm 0.14
M6	6.9 \pm 6.2	2.5 \pm 9.2	0.35 \pm 0.98	1.02 \pm 0.63	-0.39 \pm 0.57
M7	6.6 \pm 10.5	3.4 \pm 5.6	0.45 \pm 0.29	0.86 \pm 0.61	-0.20 \pm 0.55

NOTE.—For the first two columns, the errors are the standard deviation of the stars within the spectral type bin.

^a f_{FUVe}, f_{NUVe} - excess flux density from layers above the photosphere.

^bA and B are the coefficients from Equation 1

- lication, Vol. 281, ESA Special Publication
- Hauschildt, P. H., Baron, E., & Allard, F. 1997, The Astrophysical Journal, 483, 390
- Hawley, S. L., Gizis, J. E., & Reid, I. N. 1996, AJ, 112, 2799
- Jenkins, J. S., Ramsey, L. W., Jones, H. R. A., et al. 2009, ApJ, 704, 975
- King, J. R., Villarreal, A. R., Soderblom, D. R., Gulliver, A. F., & Adelman, S. J. 2003, AJ, 125, 1980
- Kraus, A. L., & Hillenbrand, L. A. 2007, AJ, 134, 2340
- Kraus, A. L., Shkolnik, E. L., Allers, K. N., & Liu, M. C. 2014, AJ, 147, 146
- Kretschmar, M., Dudok de Wit, T., Lilensten, J., et al. 2009, Acta Geophysica, 57, 42
- Lépine, S., Hilton, E. J., Mann, A. W., et al. 2013, AJ, 145, 102
- Linsky, J. L., France, K., & Ayres, T. 2013, ApJ, 766, 69
- Loyd, R. O. P., & France, K. 2014, ApJS, 211, 9
- Luger, R., & Barnes, R. 2015, Astrobiology, 15, 119
- Luger, R., Barnes, R., Lopez, E., et al. 2015, Astrobiology, 15, 57
- Luhman, K. L. 1999, ApJ, 525, 466
- Mann, A. W., Feiden, G. A., Gaidos, E., Boyajian, T., & von Braun, K. 2015, ApJ, 804, 64
- McCook, G. P., & Sion, E. M. 1999, ApJS, 121, 1
- Miguel, Y., & Kaltenegger, L. 2014, ApJ, 780, 166
- Mitra-Kraev, U., Harra, L. K., Güdel, M., et al. 2005, A&A, 431, 679
- Montes, D., López-Santiago, J., Gálvez, M. C., et al. 2001, MNRAS, 328, 45
- Morrissey, P., Schiminovich, D., Barlow, T. A., et al. 2005, ApJ, 619, L7
- Morrissey, P., Conrow, T., Barlow, T. A., et al. 2007, ApJS, 173, 682
- Newton, E. R., Charbonneau, D., Irwin, J., et al. 2014, AJ, 147, 20
- Nidever, D. L., Marcy, G. W., Butler, R. P., Fischer, D. A., & Vogt, S. S. 2002, ApJS, 141, 503

- Perryman, M. A. C., Lindegren, L., Kovalevsky, J., et al. 1997, *A&A*, 323, L49
- Rajpurohit, A. S., Reylé, C., Allard, F., et al. 2013, *A&A*, 556, A15
- Reid, I. N., & Cruz, K. L. 2002, *AJ*, 123, 2806
- Reid, I. N., Cruz, K. L., & Allen, P. R. 2007, *AJ*, 133, 2825
- Reid, I. N., Hawley, S. L., & Gizis, J. E. 1995, *AJ*, 110, 1838
- Rugheimer, S., Kaltenegger, L., Segura, A., Linsky, J., & Mohanty, S. 2015, *ApJ*, 809, 57
- Schlieder, J. E., Lépine, S., & Simon, M. 2012, *AJ*, 143, 80
- Schmidt-Kaler, T. 1982, "Physical Parameters of the Stars", Vol. 2 (Springer-Verlag, Berlin)
- Scholz, R.-D., Meusinger, H., & Jahrei, H. 2005, *A&A*, 442, 211
- Segura, A., Walkowicz, L. M., Meadows, V., Kast- ing, J., & Hawley, S. 2010, *Astrobiology*, 10, 751
- Shkolnik, E., Liu, M. C., & Reid, I. N. 2009, *ApJ*, 699, 649
- Shkolnik, E. L. 2013, *ApJ*, 766, 9
- Shkolnik, E. L., Anglada-Escudé, G., Liu, M. C., et al. 2012, *ApJ*, 758, 56
- Shkolnik, E. L., & Barman, T. S. 2014, *AJ*, 148, 64
- Shkolnik, E. L., Liu, M. C., Reid, I. N., Dupuy, T., & Weinberger, A. J. 2011, *ApJ*, 727, 6
- Shkolnik, E. L., Rolph, K. A., Peacock, S., & Bar- man, T. S. 2014, *ApJ*, 796, L20
- Short, C. I., & Hauschildt, P. H. 2005, *The Astro- physical Journal*, 618, 926
- Stelzer, B., Marino, A., Micela, G., López- Santiago, J., & Liefke, C. 2013, *MNRAS*, 431, 2063
- Tian, F., France, K., Linsky, J. L., Mauas, P. J. D., & Vieytes, M. C. 2014, *Earth and Planetary Science Letters*, 385, 22
- Torres, C. A. O., Quast, G. R., da Silva, L., et al. 2006, *A&A*, 460, 695
- Welsh, B. Y., Wheatley, J., Browne, S. E., et al. 2006, *A&A*, 458, 921
- Wheatley, J. M., Welsh, B. Y., & Browne, S. E. 2008, *AJ*, 136, 259